

NIST-GCR-93-631

**RADIATION AND MIXING PROPERTIES
OF BUOYANT TURBULENT DIFFUSION
FLAMES**

U. U. Koylu, Z. Dai, L.-K. Tseng and G. M. Faeth
University of Michigan
Ann Arbor, MI

NIST

United States Department of Commerce
Technology Administration
National Institute of Standards and Technology

NIST-GCR-93-631

RADIATION AND MIXING PROPERTIES
OF BUOYANT TURBULENT DIFFUSION
FLAMES

U. U. Koylu, Z. Dai, L.-K. Tseng and G. M. Faeth
University of Michigan
Ann Arbor, MI

October 1992
Issued July 1993



Sponsored by:
U.S. Department of Commerce
Ronald H. Brown, *Secretary*
National Institute of Standards and Technology
Arati Prabhakar, *Director*

Notice:

This report was prepared for the Laboratory of Building and Fire Research of the National Engineering Laboratory, National Institute of Standards and Technology, under Grant number 60NANB1D1175. The statements and conclusions contained in this report are those of the authors and do not necessarily reflect the views of the National Institute of Standards and Technology or the Laboratory for Building and Fire Research.

**RADIATION AND MIXING
PROPERTIES OF BUOYANT
TURBULENT DIFFUSION FLAMES**

Ü.Ö. Köylü, Z. Dai, L.-K. Tseng and G. M. Faeth
Department of Aerospace Engineering
The University of Michigan
Ann Arbor, Michigan

Prepared for:

U.S. Department of Commerce
National Institute of Standards and Technology
(formerly National Bureau of Standards)
Laboratory for Building and Fire Research
Washington, D.C. 20234

NBS Grant No. 60NANB1D1175
H. R. Baum, NIST Scientific Officer

October 1992

Abstract

An investigation of the radiation and mixing properties of buoyant turbulent diffusion flames is described, limited to processes within the fuel-lean (overfire) region. The study was divided into two phases: (1) the optical properties of soot, which are needed to interpret laser extinction measurements for soot concentrations and to compute continuum radiation from soot; and (2) the structure and mixing properties of turbulent plumes, which are needed to resolve effects of turbulence/radiation interactions and to benchmark models of these flows.

Measurements of soot optical properties were limited to the long residence time regime where soot structure is independent of both the position in the overfire region of the flame and the flame residence time. Measurements included scattering, absorption and extinction crosssections for acetylene, propylene, ethylene and propane flames burning in still air. The measurements were compared with predictions using the Rayleigh-Debye-Gans (RDG) approximation for polydisperse fractal aggregates of spherical primary soot particles having constant diameters, with aggregate structure information drawn from earlier work. The present soot aggregates exhibited significant departures from Rayleigh scattering behavior, however, the RDG polydisperse fractal aggregate theory generally provided an acceptable basis to treat their optical properties.

Measurements of turbulent mixing properties of buoyant turbulent plumes involved laser-induced iodine fluorescence to find mean and fluctuating mixture fractions. Present measurements extended to fully-developed conditions at large distances from the source of buoyancy, e.g., up to 151 source diameters and 43 Morton length scales. The results indicated that existing measurements of plume properties in the literature represent transitional plumes and that fully-developed plumes are somewhat narrower with higher levels of concentration fluctuations near the axis. Other measurements reported include probability density functions, temporal power spectra, two-point spatial correlations and temporal and spatial integral scales — all in the fully-developed turbulent plume region.

Acknowledgment

This research was supported by the United States Department of Commerce, National Institute of Standards and Technology (formerly National Bureau of Standards), Grant No. 60NANB1D1175, with H. R. Baum of the Laboratory for Building and Fire Research serving as Scientific Officer. The authors wish to acknowledge helpful discussions with R. A. Dobbins of Brown University concerning soot optical properties.

Table of Contents

	<u>Page</u>
Abstract	iv
Acknowledgments	v
List of Tables	vii
List of Figures	viii
Nomenclature: Soot Optical Properties	ix
Nomenclature: Buoyant Turbulent Plumes	xi
1. Introduction	1
2. Soot Optical Properties	2
2.1 Introduction	2
2.2 Experimental Methods	3
2.3 Theoretical Methods	5
2.4 Results and Discussion	9
2.5 Conclusions	21
3. Buoyant Turbulent Plumes	22
3.1 Introduction	22
3.2 Experimental Methods	24
3.3 Results and Discussion	30
3.4 Conclusions	
References	45

List of Tables

<u>Table</u>	<u>Title</u>	<u>Page</u>
1	Structure and optical crossection properties of overfire soot.....	10
2	Soot aggregate fractal properties from thermophoretic sampling (TS) and light scattering (LS) measurements.....	13
3	Soot aggregate size distribution properties from thermophoretic sampling and light scattering (LS) measurements	15
4	Measured and predicted extinction crossections, \bar{C}_e^a (nm ²) × 10 ⁻³ , for overfire soot aggregates.....	19
5.	Buoyant turbulent plume test conditions	29

List of Figures

<u>Figure</u>	<u>Caption</u>	<u>Page</u>
1	Sketch of overfire soot scattering apparatus.	4
2	Measured and predicted volumetric crosssections as a function of the modulus of the scattering vector.	11
3	Measured and predicted angular scattering patterns of overfire soot aggregates in turbulent acetylene/air diffusion flames.	16
4	Measured and predicted angular scattering patterns of overfire soot aggregates in turbulent ethylene/air diffusion flames.	17
5	Mean ratios of scattering to absorption crosssections as a function of wavelength for overfire soot aggregates in turbulent diffusion flames based on the predictions of the RDG polydisperse fractal aggregate theory.	20
6	Sketch of the buoyant turbulent plume apparatus.	25
7	Sketch of the two-point LIF system.	27
8	Mean mixture fractions along the plume axis.	31
9	Development of radial profiles of mean mixture fractions.	32
10	Radial profiles of mean mixture fractions in the fully-developed turbulent buoyant plume region.	33
11	Radial profiles of mixture fraction fluctuations.	35
12	Probability density functions of mixture fractions at $(x-x_0)/d = 86.7$	37
13	Temporal power spectral densities of mixture fraction fluctuations.	38
14	Radial profiles of temporal integral scales.	40
15	Symmetric and positive spatial correlations of mixture fraction fluctuations.	41
16	Negative spatial correlations of mixture fraction fluctuations.	42
17	Radial profile of spatial integral scales.	44

Nomenclature: Soot Optical Properties:

C	= optical crosssection
d_p	= primary particle diameter
D_f	= mass fractal dimension
$E(m)$	= refractive index function, $\text{Im}((m^2-1)/(m^2+2))$
$f(q, R_g)$	= aggregate form factor, equation (3)
f_{VA}, f_{VR}	= soot volume fractions from aggregate and Rayleigh theories
$F(m)$	= refractive index function $\text{Re}((m^2-1)/(m^2+2))^2$
$g(k, R_g, D_f)$	= aggregate total scattering factor, equation (7)
i	= $(-1)^{1/2}$
k	= wave number, $2\pi/\lambda$
k_f	= fractal prefactor, equation (1)
m	= refractive index of soot, $n + i\kappa$
n	= real part of refractive index of soot
n_a	= mean number of aggregates per unit volume
n_p	= mean number of primary particles per unit volume
N	= number of primary particles per aggregate
N_c	= aggregate size for onset of wide-angle regime, equation (16)
N_g	= geometric mean number of primary particles per aggregate
$p(N)$	= probability density function of aggregate size
q	= modulus of scattering vector, $2k \sin(\theta/2)$
Q	= volumetric optical crosssection
R_g	= radius of gyration of an aggregate
x_p	= primary particle size parameter, $\pi d_p/\lambda$
β	= aggregate scattering parameter, $3D_f/(8k^2 R_g^2)$
θ	= angle of scattering from forward direction
κ	= imaginary part of refractive index of soot
λ	= wavelength of radiation
ρ_{sa}	= ratio of scattering to absorption crosssection
ρ_v	= depolarization ratio
σ_g	= geometric standard deviation of aggregate size distribution
Subscripts	
a	= absorption
d	= differential
e	= extinction

h = horizontal polarization
ij = incident (i) and scattered (j) polarization direction
s = total scattering
v = vertical polarization

Superscripts

a = aggregate property
p = primary particle property
 $\bar{(\)}$ = mean value over a polydisperse aggregate population

Nomenclature: Buoyant Turbulent Plumes:

d	= source diameter
$E(n)$	= temporal power spectral density function
f	= mixture fraction
$F(r/(x-x_0))$	= radial distribution of mean mixture fractions in self-preserving regime
Fr_0	= source Froude number, $(\rho_\infty u_0^2 / (\rho_0 - \rho_\infty g d))^{1/2}$
g	= acceleration of gravity
l_M	= Morton length scale, $(\rho_\infty d u_0^2 / (g \rho_0 - \rho_\infty))^{1/2}$
n	= frequency
$PDF(f)$	= probability density function of mixture fraction
r	= radial distance
Re_0	= source Reynolds number, $u_0 d / \nu_0$
u	= streamwise velocity
x	= streamwise distance
Δr	= radial distance increment
Λ_g	= radial spatial integral scale
ν	= kinematic viscosity
ρ	= density
τ	= integral time scale

Subscripts

c	= centerline value
o	= initial value
∞	= ambient value

Superscripts

$\bar{(\)}$	= time-averaged mean value
$\overline{(\)'}$	= root-mean-squared fluctuating value

1. INTRODUCTION

An investigation is described that is relevant to two aspects of unwanted fires: (1) the emission of toxic, irritating and visibility-limiting materials like carbon monoxide and soot from fires; and (2) the emission of radiation from fires. In particular, carbon monoxide emissions are a significant cause of fatalities in fires while the presence of soot in the fuel-lean (overfire) region obscures the flaming region and hampers fire-fighting efforts and the escape of individuals from burning structures. Similarly, flame radiation is an important property of fires that influences burning rates, flame propagation rates, fire growth rates, extinguishing strategies, and the thermal stress of individuals and structures in unwanted fire environments.

The first phase of the research concerns the optical properties of soot in flames, specifically considering soot properties in the overfire region of buoyant turbulent diffusion flames. The motivation for this work is that earlier results demonstrated a strong correlation between carbon monoxide and soot emissions from flames (Köylü et al., 1991; Köylü and Faeth, 1991a,b), while continuum radiation from soot is the main radiative effect in practical fires (Köylü and Faeth, 1992a,b,c). Understanding the optical properties of soot is crucial for a better understanding of both of these problems: soot concentrations and structure generally are measured using nonintrusive laser-based methods requiring knowledge of optical properties to correctly interpret the measurements, while soot optical properties clearly have a direct bearing on the continuum radiation properties of flames. The present research involved studying the scattering, absorption and extinction properties of soot in the overfire region of buoyant turbulent diffusion flames in the long residence time regime, where soot properties are independent of both position in the overfire region and the flame residence time for a particular fuel (Köylü and Faeth, 1991a,b, 1992a; Köylü et al., 1991; Sivathanu and Faeth, 1990). The advantage of these conditions is that soot properties are universal for a particular fuel and that most practical fires are in the long residence time regime.

The second phase of the research relates to mixture fraction statistics needed to understand effects of turbulence/radiation interactions on both the mean and fluctuating radiation properties of flames. In particular, stochastic simulation techniques have been developed to estimate the effects of turbulent/radiation interactions in flames based on the laminar flamelet concept and a knowledge of mixture fraction statistics, see Kounalakis et al. (1991) and references cited therein. Unfortunately, in spite of extensive studies of scalar properties in buoyant turbulent diffusion flames and plumes, existing information on mixture fraction statistics is too limited for general use of the stochastic simulation methodology. Thus, this phase of the investigation considered mixture fraction statistics for buoyant turbulent plumes as a model of the overfire region. This problem was considered as a first step toward addressing more complex fire environments, as well as due to the fundamental importance of plume properties for understanding buoyancy-turbulence interactions that affect flow structure in flames.

The studies of soot optical properties and buoyant turbulent plumes are described, in turn, in the following. The present discussion is brief; therefore, other reports and publications concerning the investigation should be considered for more details, e.g., Kounalakis et al. (1991), Köylü (1992), Köylü and Faeth (1991a,b, 1992a,b,c) and Köylü

et al. (1991). The description of each phase of the research is sufficiently complete so that it can be read independently.

2. SOOT OPTICAL PROPERTIES

2.1 Introduction

Soot optical properties must be understood in order to estimate continuum radiation from flames and to develop nonintrusive laser-based methods for measuring soot properties. Estimating soot optical properties is challenging, however, because soot structure is complex. In particular, although soot consists of small spherical primary particles that generally satisfy the Rayleigh scattering approximation, the primary particles collect into wispy aggregates that do not exhibit either simple Rayleigh or Mie scattering behavior (Erickson et al., 1964; Dalzell et al., 1970; Wersborg et al., 1973; Magnussen, 1974). In spite of the complexities, however, potentially effective theories of soot optical properties have been developed based on mass fractal concepts, see Jullien and Botet (1987), Martin and Hurd (1987), Dobbins and Megaridis (1992) and references cited therein. Nevertheless, these methods have not been directly evaluated at conditions where both soot structure and optical properties are known (Köylü and Faeth, 1992b). Thus, the objective of the present investigation was to undertake such an evaluation by completing measurements of soot optical properties at conditions where Köylü and Faeth (1992a) had recently completed measurements of soot structure. In addition, the existing theories were extended in order to resolve problems disclosed by the present evaluation.

The soot structure measurements of Köylü and Faeth (1992a) were carried out in the fuel-lean (overfire) region of buoyant turbulent diffusion flames burning in still air within the long residence time regime. These conditions are of interest because overfire soot aggregates are large, providing a stringent test of theories of soot optical properties. Additionally, soot structure for a particular fuel in the long residence time regime is independent of position in the overfire region and residence time, which both simplifies measurements of optical properties and provides results of some general interest for studies of flame radiation. The structure measurements were carried out by thermophoretic sampling and analysis using transmission electron microscopy (TEM). The findings include fractal dimensions, and the probability density distributions of primary particle diameters and the number of primary particles in aggregates, for a variety of gaseous and liquid fuels. Present measurements included scattering, absorption and extinction crosssections at 514.5 nm, and extinction crosssections at 632.8 and 1152 nm, for flames fueled with acetylene, propylene, ethylene and propane.

The discussion begins with descriptions of experimental and theoretical methods. This is followed by results, considering estimates of soot structure parameters from scattering measurements, angular scattering patterns and extinction properties, in turn. The present discussion is brief, additional details and a complete tabulation of data can be found in Köylü (1992).

2.2 Experimental Methods

Apparatus. A sketch of the test apparatus appears in Fig. 1. The arrangement was the same as for the soot structure measurements of Köylü and Faeth (1992a) except for the presence of a soot collection system needed for the scattering measurements. Combustion was in still air with the burners located within a large enclosure ($2.4 \times 2.4 \times 3.6$ m high). The enclosure had a metal hood at the top and an adjustable exhaust system to collect and remove combustion products. The side walls of the enclosure were plastic strips to minimize effects of room disturbances. A water-cooled burner having an exit diameter of 50 mm, described by Sivathanu and Faeth (1990), was used to yield strongly buoyant, pool-like turbulent flames in the long residence time regime.

Soot optical properties were measured by collecting the combustion products in a heated hood (to prevent thermophoretic deposition of soot on the hood surfaces). The hood had a 155 mm diameter exhaust duct at the top which discharged into the main hood of the apparatus. Mixing within the heated hood was sufficient to yield uniform soot and gas species concentrations across the exit of the exhaust duct where the scattering and extinction measurements were made. Note that since soot structure is independent of position in the overfire region at long residence time conditions, collection in this manner does not affect soot structure properties.

Scattering Measurements. An argon-ion laser having an optical power of 1700 mW at 514.5 nm was used for the scattering measurements. The incident laser beam was passed through a polarization rotator and a mechanical chopper (operating at 1250 Hz) before being focused at the center of the exhaust duct using a 1000 mm focal length lens. This yielded a waist diameter of 260 μm and a confocal length of roughly 400 mm. The collecting optics were mounted on turntable surrounding the exhaust duct so that scattering angles, $\theta = 5\text{-}160^\circ$, could be considered. The collecting optics consisted of an 85 mm focal length lens, a dichroic sheet polarizer, a laser line filter (1 nm bandwidth) and a photomultiplier. The lens aperture defined a solid collection angle of 0.002 sr with a 1 mm long sampling volume at $\theta = 90^\circ$, which increased to roughly 11 mm at $\theta = 5^\circ$. Neutral density filters were used in the optical path to control the dynamic range of detection. The experimental area as well as the receiving optics were covered with black cloth to reduce optical noise from the room lighting and the flame. The detector output passed through a lock-in amplifier and was stored on a computer, sampling at 500 Hz for 10s and averaging five sampling intervals to achieve a repeatability within 10%.

The angular light scattering system was calibrated by measuring Rayleigh scattering from nitrogen gas. After correction for the $\sin^2 \theta$ dependence of the scattering volume, the vv and hh differential cross sections were within 10% of Rayleigh scattering predictions for $\theta = 5\text{-}160^\circ$. Absolute volumetric differential scattering cross sections of soot were found from ratios of the detector signal for soot and nitrogen, after accounting for signal attenuation in the optical path, based on the nitrogen optical properties of Rudder and Bach (1968). Total volumetric scattering cross sections were found by integrating the volumetric differential scattering cross sections over the whole spherical surface. This required extrapolation of the measurements to reach $\theta = 0$ and 180° , however, uncertainties caused by the extrapolations were small due to the limited solid angle involved for forward scattering and the relatively slow variation of scattering with θ in the backward direction. The overall experimental uncertainties (95% confidence) of

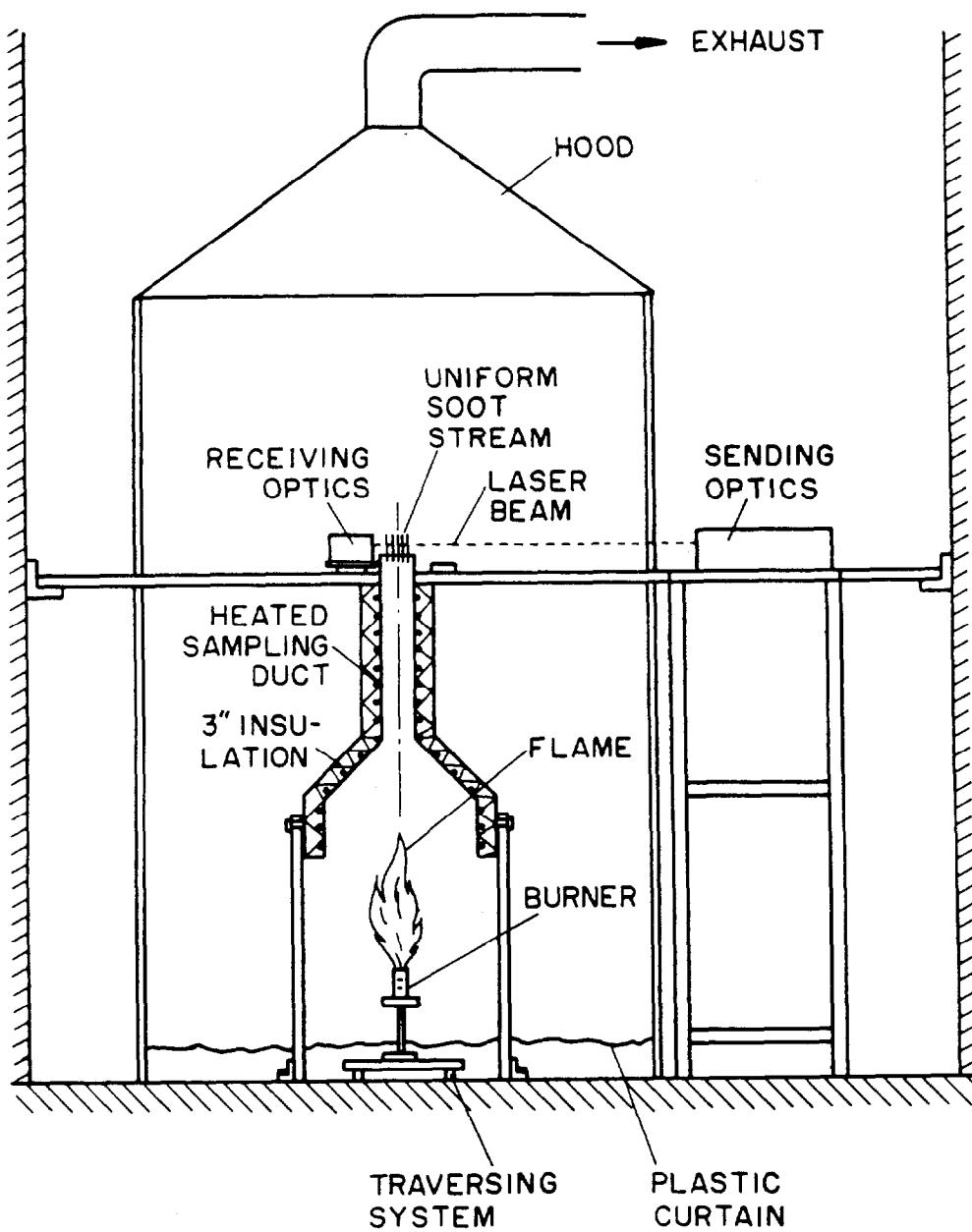


Figure 1. Sketch of overfire soot scattering apparatus

the angular and the total light scattering measurements were comparable and were estimated to be less than 20%, dominated by finite sampling times, the finite aperture of the detector and the angular uncertainty of the collecting optics.

Extinction Measurements. Volumetric extinction cross sections were measured at 514.5 nm using the argon-ion laser, and at 632.8 and 1152 nm using 15 and 40 mW HeNe lasers, respectively. Laser power meters were used to measure the intensity of the beams before and after crossing the 155 mm long path through the exhaust flow. The extinction ratio was found by sampling at 500 Hz for 20s and averaging five sampling intervals to achieve a repeatability within 5%. Experimental uncertainties (95% confidence) of these measurements were generally less than 20%, largely controlled by the magnitude of the extinction ratio and finite sampling times. Volumetric absorption cross sections were found by subtracting the total scattering cross sections from the extinction cross sections, yielding uncertainties (95% confidence) generally less than 30%.

2.3 Theoretical Methods

General Description. Predictions of soot optical properties were based on methods described by Jullien and Botet (1987), Martin and Hurd (1987) and Dobbins and Megaridis (1992). These methods were extended, however, to improve the treatment of polydisperse aggregate populations in view of the large size and broad size distributions of the present overfire soot. Major assumptions with respect to aggregate structure are as follows: spherical primary particles having constant diameters, primary particles just touch one another, uniform refractive indices, log-normal aggregate size distributions and the aggregates are mass fractal-like objects. The mass fractal approximation implies the following relationship between the number of particles in an aggregate and its radius of gyration (Jullien and Botet, 1987):

$$N = k_f (R_g/d_p)^{D_f} \quad (1)$$

The assumptions of nearly constant diameter spherical primary particles, log-normal size distributions and mass fractal-like behavior are justified by the soot structure measurements for present conditions (Köylü and Faeth, 1992a). The remaining assumptions are typical of past treatments of soot optical properties, see Köylü and Faeth (1992b) and references cited therein.

Scattering was found using the Rayleigh-Debye-Gans (RDG) approximation where effects of multiple- and self-scattering are ignored so that the electric field of each primary particle is the same as the incident electric field, and differences of the phase shift of scattered light from various points within a particular primary particle are ignored. RDG scattering requires that both $|m-1| \ll 1$ and $2x_p |m-1| \ll 1$ (Kerker, 1969; van de Hulst, 1957; Bohren and Huffman, 1983), which is questionable for soot aggregates due to the relatively large refractive indices of soot. In addition, recent computational studies suggest significant effects of multiple scattering for aggregates typical of overfire soot, see Berry and Percival (1986), Chen et al. (1990), Ku and Shim (1992) and Nelson (1989). Thus, use of RDG theory only can be justified by its capabilities to treat measured soot optical properties effectively, which was the main motivation for the present investigation.

Single Aggregates. Under the present approximations, individual primary particles satisfy the Rayleigh scattering approximation, yielding the following expressions for their optical properties (Bohren and Hoffman, 1983; Kerker, 1969):

$$C_a^p = 4\pi x_p^3 E(m)/k^2, C_s^p = 8\pi x_p^6 F(m)/(3k^2), C_{vv}^p = x_p^6 F(m)/k^2 \quad (2)$$

where $C_{hv}^p = C_{vh}^p \approx 0$, $C_{hh}^p = C_{vv}^p \cos^2 q$ and $C_e^p = C_a^p + C_s^p$. The cross sections in equations (2) will be used in the following to normalize aggregate optical cross sections. The treatment of aggregate optical properties will begin with the scattering cross sections found for fractal aggregates under the RDG approximation by Dobbins and Megaridis (1992):

$$C_{vv}^a(\theta) = C_{hh}^a(\theta)/\cos^2 q = N^2 C_{vv}^p f(q R_g) \quad (3)$$

where the form factor, $f(q R_g)$, is expressed as follows in the Guinier (small-angle) and large-angle regimes, respectively:

$$f(q R_g) = \exp(-(q R_g)^2/3), \quad (q R_g)^2 \leq 3D_f/2 \quad (4)$$

$$f(q R_g) = (q R_g)^{-D_f}, \quad (q R_g)^2 > 3D_f/2 \quad (5)$$

Within present approximations, $C_{hv}^a = C_{vh}^a = 0$ so that the differential scattering cross section for unpolarized light becomes:

$$C_d^a(\theta) = (C_{vv}^a(\theta) + C_{hh}^a(\theta))/2 = C_{vv}^a(\theta) (1 + \cos^2 \theta)/2 \quad (6)$$

The total scattering cross section can be found by integrating equation (6) over the whole spherical surface to yield:

$$C_s^a = C_s^p N^2 g(k, R_g, D_f) \quad (7)$$

The aggregate total scattering factor, $g(k, R_g, D_f)$, takes on different forms depending on whether the large-angle regime is reached for $\theta \leq 180^\circ$, as follows:

$$g(k, R_g, D_f) = 1 - 2(k R_g)^2/3, \quad (k R_g)^2 \leq 3D_f/8 \quad (8)$$

$$g(k, R_g, D_f) = \frac{\beta}{2} (3 - 3\beta + 2\beta^2) - \frac{(k R_g \beta)^2}{3} (3 - 4\beta + 3\beta^2) + (2k R_g)^{-D_f}$$

$$\left[\frac{3}{2-D_f} - \frac{12}{(6-D_f)(4-D_f)} - 3\beta^{1-D_f/2} \left(\frac{1}{2-D_f} - \frac{2\beta}{4-D_f} + \frac{2\beta^2}{6-D_f} \right) \right], \quad (k R_g)^2 > 3D_f/8 \quad (9)$$

At this point, the present treatment departs from Dobbins and Megaridis (1992), which was limited to the Guinier regime, i.e., equation (8).

Based on the simulations of Nelson (1989) and Chen et al. (1990), it is assumed that absorption is not affected by aggregation, yielding

$$C_a^a = N C_a^p \quad (10)$$

The extinction cross section is the sum of the absorption and scattering cross sections, i.e.,

$$C_e^a = C_a^a + C_s^a = N C_a^p (1 + \rho_{sa}^a) \quad (11)$$

where

$$\rho_{sa}^a = \rho_{sa}^p Ng(k, R_g, D_f) \quad (12)$$

The parameters ρ_{sa}^p and ρ_{sa}^a are the ratio of scattering to absorption cross sections for primary particles and aggregates, respectively. For aggregates, ρ_{sa}^a represents the error in soot volume fraction determinations when extinction measurements are processed using the Rayleigh scattering approximation (which implies $\rho_{sa}^a \approx 0$). At the limit of large aggregates, ρ_{sa}^a saturates to a value that is independent of N , where equations (9) and (12), yield:

$$\rho_{sa}^a = \rho_{sa}^p k_f (4x_p)^{-D_f} (3/(2-D_f) - 12/((6-D_f)(4-D_f))) \quad (13)$$

This behavior is fundamentally different from Mie scattering for an equivalent spherical aggregate, where ρ_{sa}^a continues to increase as N increases, as discussed by Berry and Percival (1986), Nelson (1989) and Dobbins and Megaridis (1992).

Polydisperse Aggregate Populations. The mean optical cross sections of populations of randomly oriented polydisperse aggregates (polydisperse aggregates) are found by integrating over all aggregate sizes, as follows:

$$\bar{C}_j^a = \int_{N=1}^{\infty} C_j^a(N) p(N) dN; \quad j = pp, s, a \quad (14)$$

where $p(N)$ is the log-normal size distribution function from Köylü and Faeth (1992a). Continuing the assumption that $C_{hv}^a = C_{vh}^a \approx 0$, the expression for the differential scattering cross sections of polydisperse aggregates becomes

$$\begin{aligned} \bar{C}_{vv}^a(\theta)/C_{vv}^p &= \bar{C}_{hh}^a(\theta)/(C_{vv}^p \cos^2\theta) = \int_{N=1}^{N_c} N^2 \exp(-q^2 R_g^2/3) p(N) dN \\ &+ \int_{N=N_c}^{\infty} N^2 (q R_g)^{-D_f} p(N) dN \end{aligned} \quad (15)$$

where

$$N_c = k_f (3D_f/(2q^2 d_p^2))^{D_f/2} \quad (16)$$

is the aggregate size at the matching point between the Guinier and large-angle regimes, and differs for each angle. Equation (15) must be integrated numerically for general variations of aggregate size and scattering angle, however, simple limits are obtained for the Guinier and large-angle regimes. In the Guinier regime, $p(N) \ll 1$ for $N \geq N_c$ and the contribution of the second integral in equation (15) is negligible, yielding (Guinier and Fournet, 1955):

$$\bar{C}_{vv}^a(\theta)/(\bar{N}^2 C_{vv}^p) = 1 - q^2 \bar{R}_g^2/3 + \dots = \exp(-q^2 \bar{R}_g^2/3), \quad \text{Guinier regime} \quad (17)$$

where

$$\bar{R}_g^2 = \frac{\int_{N=1}^{\infty} R_g(N)^2 N^2 p(N) dN}{\int_{N=1}^{\infty} N^2 p(N) dN}, \quad \text{Guinier regime} \quad (18)$$

In the large-angle regime, $p(N) \ll 1$ for $N \leq N_c$ and the contribution of the first integral in equation (15) is negligible, yielding (Köylü, 1992):

$$\bar{C}_{vv}^a(\theta)/C_{vv}^p = \bar{N} k_f (q d_p)^{-D_f} = \bar{N}^2 (q^2 \bar{R}_g^2)^{-D_f/2}, \quad \text{large-angle regime} \quad (19)$$

where

$$\bar{R}_g^2 = \left[\frac{\int_{N=1}^{\infty} R_g(N)^{2D_f} p(N) dN}{\int_{N=1}^{\infty} R_g(N)^{D_f} p(N) dN} \right]^{2/D_f}, \quad \text{large-angle regime} \quad (20)$$

The difference between the mean square radius of gyration in the Guinier and large-angle regimes is expected because large aggregates dominate scattering at small angles while small aggregates contribute more to the scattering pattern at large angles. Thus, using one definition for \bar{R}_g^2 at all scattering angles is not correct. Furthermore, at any angle, some of the aggregates are in the Guinier regime while others are in the large-angle regime; thus, the crossover between small-and large-angle behavior is more gradual for polydisperse aggregate populations than for individual aggregates.

The total scattering cross section of polydisperse aggregates is found from equations (7) and (14) as follows:

$$\bar{C}_s^a = C_s^p \int_{N=1}^{\infty} N^2 g(k, R_g, D_f) p(N) dN \quad (21)$$

Equation (21) must be numerically integrated, using equation (1) to relate R_g and N , after substituting for $g(k, R_g, D_f)$ from equations (8) and (9) and introducing the log-normal function for $p(N)$.

The absorption cross section of polydisperse aggregates can be evaluated easily from equations (10) and (14), as follows:

$$\bar{C}_a^a = \bar{N} C_a^p \quad (22)$$

Similar to a single aggregate, the extinction cross section can be written in terms of the ratio of scattering to absorption cross sections, $\bar{\rho}_{sa}^a = \bar{C}_s^a/\bar{C}_a^a$, to yield:

$$\bar{C}_e^a = \bar{N} C_a^p (1 + \bar{\rho}_{sa}^a) \quad (23)$$

where $\bar{\rho}_{sa}^a$ reduces to ρ_{sa}^a from equation (13) at the limit of large monodisperse aggregates.

2.4 Results and Discussion

Optical Cross Sections. The measured volumetric optical cross sections were converted to optical cross sections using the approximation that absorption is not affected by aggregation. Then the number of primary particles per unit volume, n_p , can be computed from

$$n_p = \bar{Q}_a^a / C_a^p \quad (24)$$

C_a^p was found from equation (2), given d_p from the structure measurements, and adopting the refractive indices of Dalzell and Sarofim (1969), i.e., $m = 1.57 + 0.56i$ at 514.5 and 632.8 nm and $1.65 + 0.75i$ at 1152 nm. The Dalzell and Sarofim (1969) refractive indices were used to be consistent with Köylü and Faeth (1992a), however, they also are preferred based on the present scattering measurements, as discussed later. Then, given \bar{N} from the soot structure measurements, the mean number of aggregates per unit volume, n_a , can be found from

$$n_a = n_p / \bar{N} \quad (25)$$

yielding the optical cross sections as follows:

$$\bar{C}_j^a(\theta) = \bar{Q}_j^a(\theta) / n_a; \quad j = pp, s, a \quad (26)$$

Soot Structure Parameters. Reference soot structure and optical cross section properties at 514.5 nm are summarized in Table 1 for the four fuels. The table also includes the primary particle properties and the values of \bar{N} that were used to find the optical cross sections of aggregates, as well as the resulting values of n_p and n_a . At 514.5 nm, x_p is in the range 0.183-0.287 which marginally places the primary particles in the Rayleigh scattering regime (Kerker, 1969). The values of $\bar{\rho}_{sa}^a$ are roughly two orders of magnitude larger than ρ_{sa}^p , highlighting the much greater degree of scattering from aggregates than from individual primary particles. As discussed earlier, $\bar{\rho}_{sa}^a$ can be viewed as the error made when soot volume fractions are computed from laser extinction measurements using the small particle (Rayleigh) scattering limit. The results of Table 1 show that this practice causes errors of 22-41% for present conditions, increasing with increasing tendency of the fuel to soot. Nevertheless, it seems premature to correct earlier measurements of soot volume fractions at the same conditions (Sivathanu and Faeth, 1990) because current uncertainties of soot refractive indices can affect these results to a much larger extent, e.g., by roughly a factor of two (Dobbins and Megaridis, 1992).

Measured and predicted values of $\bar{Q}_{vv}^a(\theta)$ are plotted as a function of qd_p at 514.5 nm in Fig. 2 for the four fuels. Extrapolations of large-angle behavior also are shown on the plots for reference purposes. The substantial departure from Rayleigh scattering behavior (where $\bar{Q}_{vv}^a(\theta)$ would be independent of qd_p) is evident, with forward scattering roughly 100 times larger than large-angle scattering for all the fuels. The large size of the present soot aggregates, and the extended transition between the Guinier and large-angle regimes due to polydisperse effects, prevented fully reaching the Guinier regime even though scattering angles as small as 5° were considered. However, the measurements provide an extended range within the large-angle regime, e.g., roughly $qd_p > 0.1$.

Table 1 Structure and optical cross section properties of overfire soot^a

Fuel	Acetylene	Propylene	Ethylene	Propane
<u>Primary Particles:</u>				
d_p (nm)	47	41	32	30
x_p (-)	0.287	0.250	0.195	0.183
C_{VV}^P (nm ² /sr)	0.814	0.359	0.0811	0.0551
C_s^P (nm ²)	6.82	3.01	0.679	0.462
C_e^P (nm ²)	524	346	164	134
r_{sa}^P (-)	0.0132	0.0088	0.0042	0.0034
n_p (mm ⁻³) × 10 ⁻⁶	6.2	6.4	2.6	2.5
<u>Aggregates:</u>				
\bar{N} (-)	417	400	467	364
\bar{C}_{VV}^a (90°) (nm ² /sr)	3710	2370	1020	559
\bar{C}_s^a (nm ²) × 10 ⁻³	92.9	55.0	21.8	10.4
\bar{C}_e^a (nm ³) × 10 ⁻³	321	194	98.2	58.8
$\bar{\rho}_{sa}^a$ (-)	0.41	0.40	0.29	0.22
$\bar{\rho}_V^a$ (-)	0.041	0.033	0.028	0.022
n_a (mm ⁻³) × 10 ⁻³	14	16	5.5	6.8

^aFor buoyant turbulent diffusion flames in still air at long residence times with optical properties at 514.5 nm: structure properties from Köylü and Faeth (1992a); soot refractive indices used in the computations from Dalzell and Sarofim (1969).

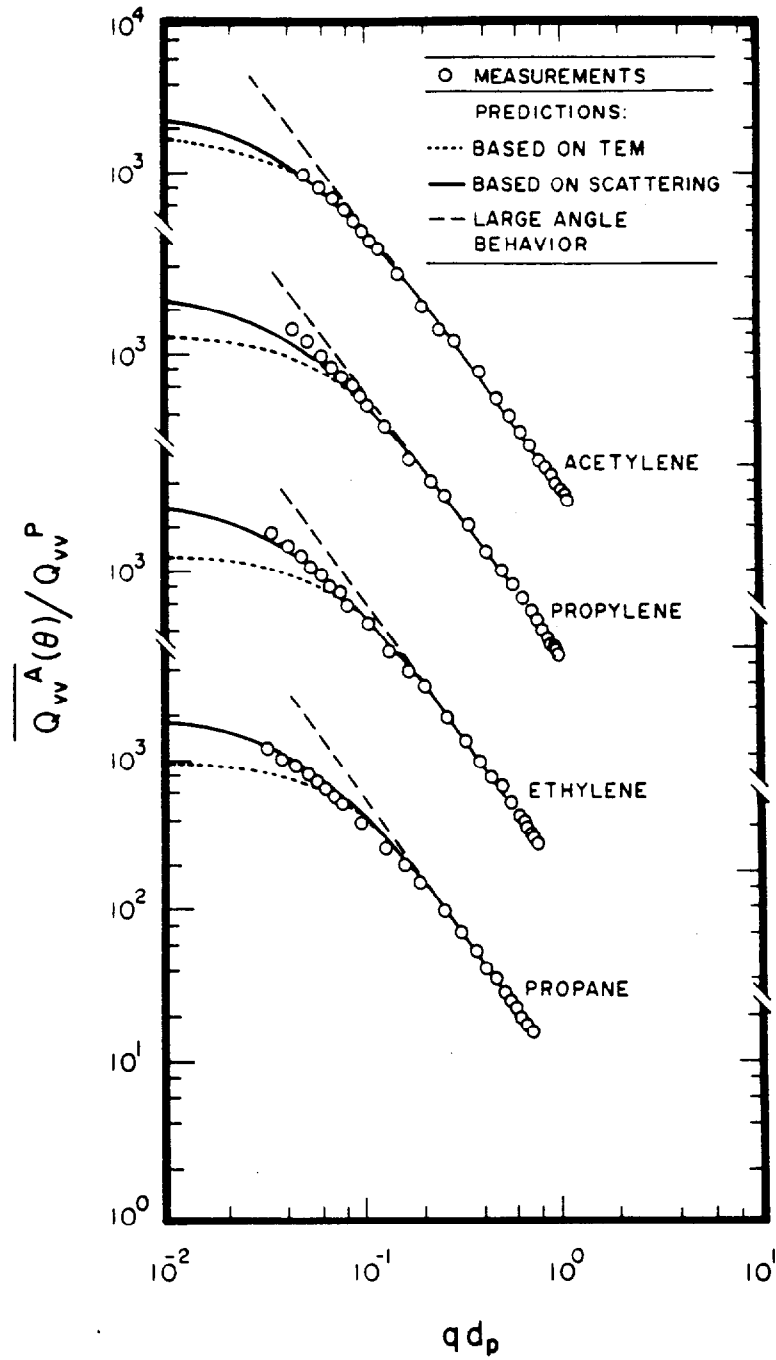


Figure 2. Measured and predicted volumetric crosssections as a function of the modulus of the scattering vector

The measurements in the large-angle regime in Fig. 2 can be interpreted to yield information about the fractal properties and the refractive indices of the present overfire soot. At large angles, through equations (19) and (26), the slope and magnitude of plots of $\bar{Q}_{vv}^a(\theta)$ as a function of $q d_p$ yield D_f and k_f . These values are summarized Table 2 for the four fuels, along with values found from the structure measurements using thermophoretic sampling and analysis with TEM. The values of D_f from the structure measurements of Köylü and Faeth (1992) and the present scattering measurements agree within experimental uncertainties and exhibit little variation with fuel type, yielding average values of 1.82 and 1.79 with standard deviations of 0.04 and 0.05, for the scattering measurements and over all the measurements. The fact that $D_f < 2$ implies fractal aggregate scattering behavior with scattering properties saturating when N is large, as suggested by equation (13), rather than Mie scattering for an equivalent sphere where ρ_{sa}^a continues to increase as N increases (Berry and Percival, 1986). Thus, aggregate sizes preclude Rayleigh scattering behavior while aggregate fractal dimensions preclude treating sizes effects by Mie scattering for an equivalent sphere. The variations of k_f with fuel type also are relatively small, yielding a mean value of 8.1 with a standard deviation of 0.8 over all the fuels. The present values of k_f are similar to the values found by Puri et al. (1992) of 9.2 and 8.6 for acetylene and ethylene flames from thermophoretic sampling measurements. Thus, both D_f and k_f appear to be relatively independent of fuel type for overfire soot aggregates.

Information about refractive indices can be obtained from the measurements in the large-angle regime by finding $\bar{Q}_{vv}^a(\theta)/\bar{Q}_a^a$ from equations (19) and (22) and eliminating C_{vv}^p and C_a^p from this expression using equation (2). After rearranging, the following expression is obtained:

$$F(m)/E(m) = 4\pi(q d_p)^{D_f} \bar{Q}_{vv}^a(\theta) / (k_f x_p^3 \bar{Q}_a^a) \quad (27)$$

All the quantities on the right hand side of equation (27) are known from either the structure or large-angle scattering measurements: d_p and x_p are summarized in Table 2; $D_f = 1.8$ and $k_f = 9.0$ are reasonable averages for present test conditions, based on the thermophoretic sampling results of Köylü and Faeth (1992a) and Puri et al. (1992); while the values of \bar{Q}_a^a are known from the present optical measurements. Then introducing $\bar{Q}_{vv}^a(\theta)$ at $\theta = 160^\circ$, which is well within the large-angle regime, yields $F(m)/E(m) = 0.74$ with a standard deviation of 0.09 over all the fuels. Available values of refractive indices at this wavelength include $m = 1.57 + 0.56i$ (Dalzell and Sarofim, 1969), $1.90 + 0.55i$ (Tien and Lee, 1981) and $1.72 + 0.60i$ (Chang and Charalampopoulos, 1990), yielding $F(m)/E(m) = 0.84, 1.55$ and 1.10 , respectively. Thus, the measurements of Dalzell and Sarofim (1969) are most consistent with present soot aggregate scattering measurements. These results also suggest that $F(m)/E(m)$ is relatively independent of fuel type for present conditions.

Two predictions based on the RDG polydisperse fractal aggregate theory are illustrated in Fig. 2, one entirely based on results from the structure (TEM) measurements, the other based on refitted aggregate size distributions (keeping \bar{N} the same) which best match the scattering measurements. Both predictions use $D_f = 1.8$ and the individual k_f values for each fuel summarized in Table 2 for the light scattering measurements. Since the predictions for each fuel use the same \bar{N} , they yield identical results in the large-angle regime through equation (19); they also are in good agreement

Table 2 Soot aggregate fractal properties from thermophoretic sampling (TS) and light scattering (LS) measurements^a

Fuel	D_f		k_f	
	TS	LS	TS ^b	LS ^c
Acetylene	1.79	1.85	9.2	7.0
Propylene	1.75	1.84	—	8.6
Ethylene	1.73	1.83	8.6	8.8
Propane	1.74	1.77	—	8.0

^aFor overfire soot from buoyant turbulent diffusion flames in still air at long residence times; light scattering measurements from the large-angle regime at 514.5 nm.

^bFrom Puri et al. (1992).

^cBased on the soot refractive indices of Dalzell and Sarofim (1969).

with the measurements in this regime. However, predictions based on the structure measurements significantly underestimate scattering levels as the Guinier regime is approached. This is plausible due to the sampling limitations of the TEM measurements, where large aggregates that dominate forward scattering might not be found in sufficient quantities. In particular, the moment ratio \bar{N}^2 , which is crucial for scattering properties in the Guinier regime (see equation (17)), exhibited large uncertainties, 40-90%, suggesting potential sampling difficulties (Köylü and Faeth, 1992a). Thus, the aggregate size distribution functions were refitted, keeping \bar{N} constant for each fuel as noted earlier, to achieve the reasonably good match of measured scattering properties in the near-Guinier regime illustrated in Fig. 2. The original and refitted aggregate size distribution parameters are summarized in Table 3 for all the fuels: changes of N_g and σ_g are within experimental uncertainties while the main difference between the thermophoretic sampling and scattering measurements is the higher order moment, \bar{N}^2 , which easily is biased during TEM measurements due to sampling limitations, e.g., only a few large aggregates can change this moment substantially. This suggests that the RDG polydisperse fractal aggregate theory provides a reasonable basis to treat overfire soot aggregates, however, additional study of the Guinier regime is needed to definitively evaluate the approach.

Angular Scattering Patterns. Predicted and measured angular scattering patterns at 514.5 nm are plotted in Figs. 3 and 4 for acetylene and ethylene as examples of strongly and weakly sooting fuels; results for propylene and propane were similar, see Köylü (1992). The predictions of $\bar{C}_{vv}^a(\theta)$ are based on the refitted soot structure properties from the light scattering measurements, and are in excellent agreement with the measurements as discussed in connection with Fig. 2. These results clearly show very strong scattering at small values of q . The formulations for hh, vh and hv scattering cross sections were modified slightly to account for observed depolarization effects. This was done by introducing depolarization ratios for soot aggregates, $\bar{\rho}_v^a$, analogous to Rayleigh scattering theory (Rudder and Bach, 1968), as follows:

$$\bar{C}_{hh}^a(\theta) = \bar{C}_{vv}^a(\theta) [(1 - \bar{\rho}_v^a) \cos^2 \theta + \bar{\rho}_v^a] \quad (28)$$

$$\bar{C}_{hv}^a = \bar{C}_{vv}^a = \bar{C}_{vv}^a(90^\circ) \bar{\rho}_v^a \quad (29)$$

The measured values of $\bar{\rho}_v^a$ are summarized in Table 1; they increase with increasing propensity of the fuel to soot and generally are an order of magnitude larger than values found for Rayleigh scattering from molecules (Rudder and Bach, 1968). The resulting predictions of $\bar{C}_{hh}^a(\theta)$ are excellent, similar to $\bar{C}_{vv}^a(\theta)$. The predicted and measured scattering cross sections for the vh and hv components also are in good agreement with Rayleigh scattering ideas, except near the forward-scattering direction where the measured values increase and the vh and hv components no longer are equal. This behavior may be caused by experimental difficulties because uncertainties increase for both the vh and hv scattering components in the forward scattering direction due to effects of polarization vector misalignment when scattering is strong. In particular, experimental problems are suggested in this region because there is no fundamental reason for the vh and hv scattering components to differ for randomly oriented aggregates of small primary particles. However, the behavior also may reflect limitations of the RDG theory due to effects of multiple scattering in the forward direction. Thus, additional theoretical consideration of the depolarization ratios of soot aggregates would be

Table 3 Soot aggregate size distribution properties from thermophoretic sampling (TS) and light scattering (LS) measurements^a

Fuel	N_g		σ_g		\bar{N}^2/\bar{N}	
	TS	LS	TS	LS	TS	LS
Acetylene	214	180	3.3	3.8	1330	1840
Propylene	227	162	3.0	3.9	1200	2860
Ethylene	290	189	2.7	3.9	1130	2390
Propane	224	162	2.9	3.6	930	2300

^aFor overfire soot from buoyant turbulent diffusion flames in still air at long residence times; light scattering measurements from near-Guinier regime at 514.5 nm. Light scattering measurements based on the soot refractive indices of Dalzell and Sarofim (1969); \bar{N} for each fuel the same for both TS and LS measurements.

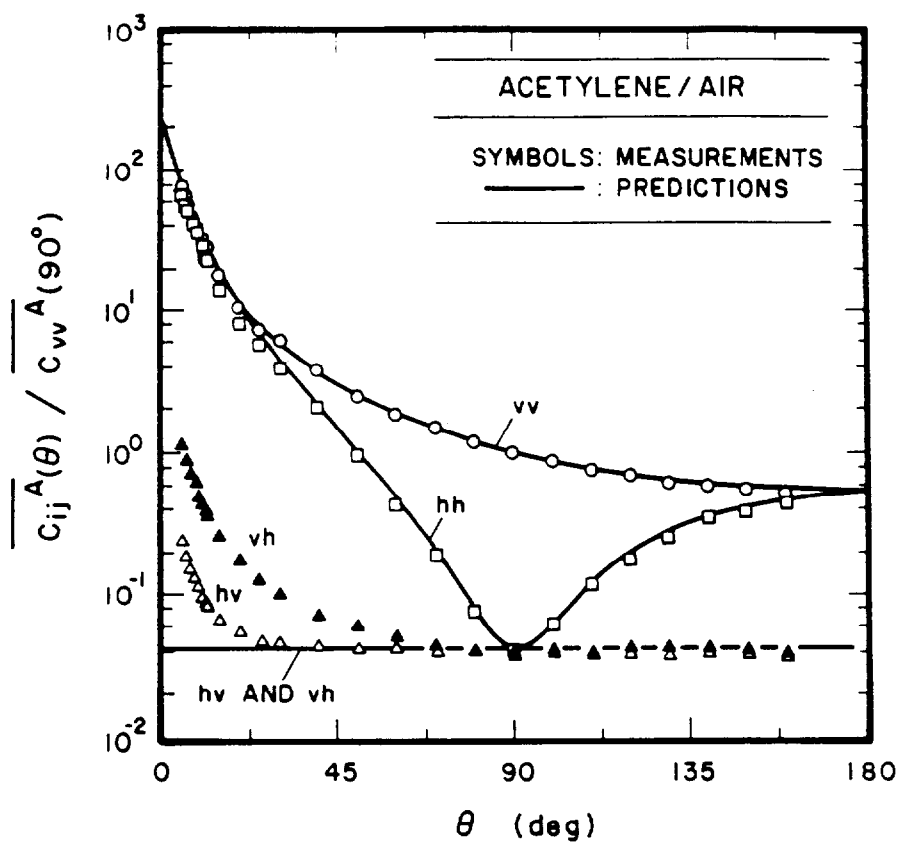


Figure 3. Measured and predicted angular scattering patterns of overfire soot aggregates in turbulent acetylene/air diffusion flames

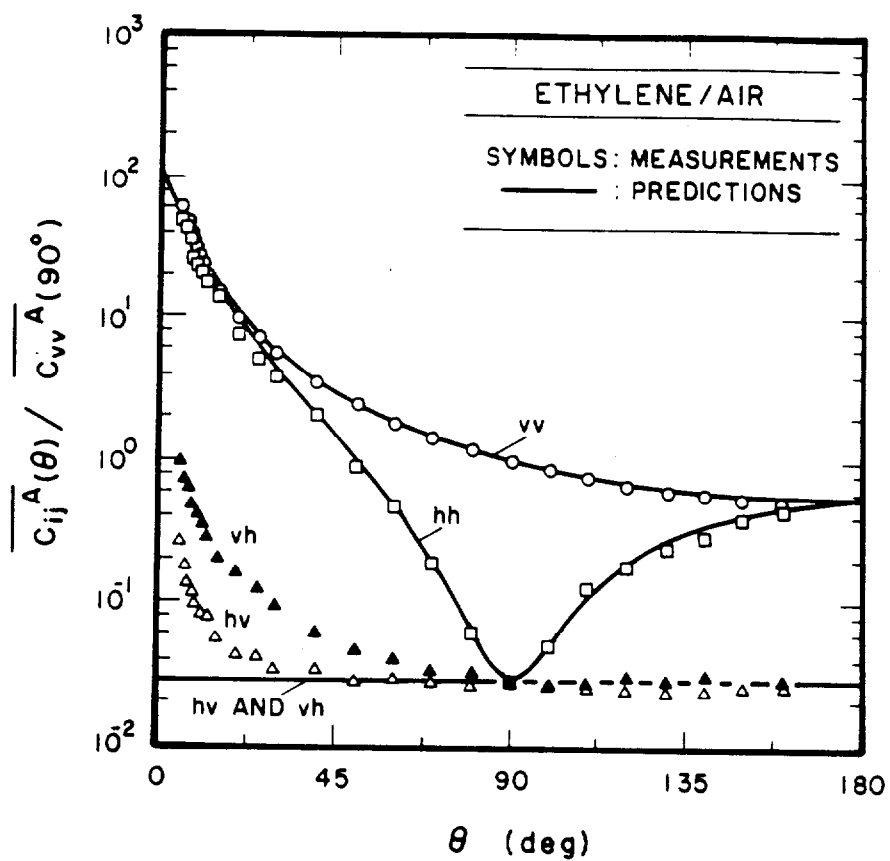


Figure 4. Measured and predicted angular scattering patterns of overfire soot aggregates in turbulent ethylene/air diffusion flames

interesting to help assess both the experimental and theoretical limitations of present methods. As a practical matter, however, the v_h and h_v components are small in comparison to v_v and h_h scattering and can be neglected for typical scattering calculations.

Extinction at Various Wavelengths. Extinction cross sections at 514.5, 632.8 and 1152 nm were measured in order to evaluate the capabilities of the RDG polydisperse fractal aggregate theory to estimate optical cross sections at various wavelengths. The results of these measurements and predictions are summarized in Table 4. The predictions are based on $D_f = 1.8$, $k_f = 8.1$ as reasonable averages of present estimates of fractal properties from Table 2, the aggregate size distribution properties from the scattering data summarized in Table 3, and the refractive indices of Dalzell and Sarofim (1969) listed earlier. Measured and predicted extinction cross sections at 514.5 nm are in close agreement but this is not very significant because soot structure and optical properties were matched at this condition. Nevertheless, predicted extinction cross sections are within 18% of the measurements at both 632.8 and 1152 nm, with the largest errors exhibited for heavily sooting fuels like acetylene and propylene; this is good agreement in view of the uncertainties of soot refractive indices.

The present RDG polydisperse fractal aggregate theory was used to estimate the scattering contribution to extinction at other wavelengths since the predictions were reasonably good at the wavelengths where measurements were made. The predicted ratios of scattering to absorption cross sections are illustrated as a function of wavelength in Fig. 5. Results are shown for both the gaseous and liquid fuels studied by Köylü and Faeth (1992a), using $D_f = 1.8$ and $k_f = 8.1$ as before. The soot aggregate size distribution parameters (N_g and σ_g) for these calculations were drawn from the thermophoretic sampling measurements of Köylü and Faeth (1992a), even though present scattering measurements for gaseous fuels suggested the need for adjusting these parameters somewhat, see Table 3. This is justified because total scattering predictions using the thermophoretic sampling measurements agreed with present measurements within 15%, because the changes of the size distribution parameters only affected results at very small angles. The predictions are presented as $\bar{\rho}_{sa}^a E(m)/F(m)$ to avoid complications due to the considerable uncertainties of soot refractive indices discussed earlier. The plot of Fig. 5 updates results reported by Köylü and Faeth (1992a), based on the RDG polydisperse fractal aggregate theory of Dobbins and Megaridis (1992), which is mainly designed to treat the Guinier regime as discussed earlier: there are quantitative differences between the two sets of the results but the general trends are similar.

The plots of $\bar{\rho}_{sa}^a$ in Fig. 5 indicate departure of aggregate scattering properties from the small particle (Rayleigh) scattering limit. The results show that this departure is greatest for strongly sooting fuels like toluene, benzene and acetylene in the visible portion of the spectrum. Noting that $F(m)/E(m)$ is of order unity, soot volume fractions would be overestimated by 20-50% for laser extinction measurements at 632.8 nm, analyzed using the Rayleigh scattering approximation. The value of $\bar{\rho}_{sa}^a$, however, decreases with increasing wavelength and becomes relatively small for wavelengths greater than 2000 nm. Thus, the effect of aggregate scattering appears to be reasonably small for estimates of soot radiation properties in the infrared, in view of other uncertainties of such calculations, even for the present rather large overfire soot aggregates.

Table 4 Measured and predicted extinction cross sections, \bar{C}_e^a (nm²) $\times 10^{-3}$, for overfire soot aggregates^a

Fuel	Acetylene	Propylene	Ethylene	Propane
<u>514.5 nm:</u>				
Measured	321	194	98.2	58.8
Predicted ^b	321	194	98.2	59.3
<u>632.8 nm:</u>				
Measured	290	172	73.1	43.7
Predicted ^b	248	143	74.7	46.5
<u>1152 nm:</u>				
Measured	176	86.8	45.5	26.9
Predicted ^b	144	84.4	45.3	28.4

^aFor buoyant turbulent diffusion flames in still air at long residence times.

^bBased on the laser scattering properties of soot aggregates fitted at 514.5 nm and the soot refractive indices of Dalzell and Sarofim (1969).

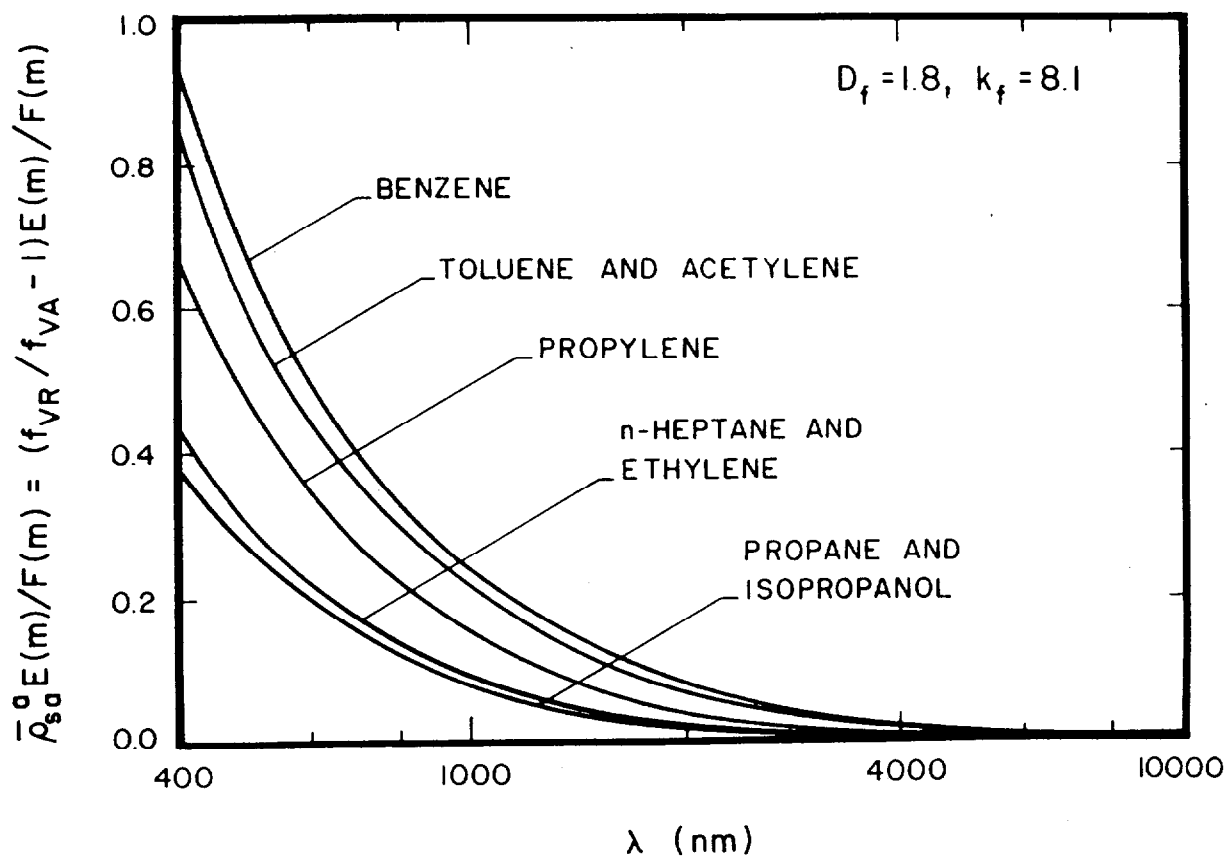


Figure 5. Mean ratios of scattering to absorption crosssections as a function of wavelength for overfire soot aggregates in turbulent diffusion flames based on the predictions of the RDG polydisperse fractal aggregate theory

Discussion. The reasonably good overall comparison between predictions using the RDG polydisperse fractal aggregate theory and the present measurements is promising. However, the evaluation was limited with respect to the general effectiveness of the RDG scattering approximation for treating soot optical properties. First of all, the large size of the present aggregates implied that the bulk of the measurements were in the large-angle regime. In this regime, the computations of Nelson (1989) suggest that effects of multiple scattering are relatively small, and that the RDG approximation of equation (5) is satisfactory even for large aggregates. Thus, while it is encouraging that predictions based solely on structure measurements were satisfactory in this regime, this does not constitute a definitive evaluation of the RDG approximation for soot aggregates.

Effects of multiple scattering are most significant for forward scattering in the Guinier regime — which would provide a strong test of the RDG scattering approximation. Unfortunately, two difficulties were encountered during the present of evaluation of predictions in this regime. First of all, the large size of the present aggregates precluded fully reaching the Guinier regime for experimentally accessible scattering angles so that the full effect of potential multiple scattering was not observed. Secondly, it was necessary to refit the aggregate size distribution function, to increase the higher moment \bar{N}^2 , in order to match the scattering data. While such refitting is plausible due to the sampling limitations of the structure measurements, as discussed earlier, the refitting also could mask fundamental deficiencies of the RDG scattering approximation. Thus, while it is encouraging that the RDG polydisperse fractal aggregate approach seems capable of correlating the present measurements of soot optical properties, and scattering measurements eventually may prove to be the best way to find the higher moments of soot aggregate size distributions, additional evaluation of the RDG approximation is needed. This will require measurements of both structure and optical properties for soot populations having smaller aggregates and thus a more extensive Guinier regime.

2.5 Conclusions

The optical properties of overfire soot were measured for buoyant turbulent diffusion flames burning in still air. The fuels considered included acetylene, propylene, ethylene and propane. Measurements were limited to the long residence time regime where soot structure was known from earlier measurements (Köylü and Faeth, 1992a), and is independent of position and residence time in the overfire region. The combined soot structure and optical property measurements were used to evaluate an approximate RDG polydisperse fractal aggregate theory of soot optical properties. The main conclusions of the study are as follows:

1. The optical properties of the present soot at 514.5 nm departed significantly from Rayleigh scattering behavior: forward scattering was roughly 100 times larger than large-angle scattering, total scattering was 22-41% of absorption, and depolarization ratios were roughly an order of magnitude larger than values typical of Rayleigh scattering from molecules. This causes soot volume fractions to be overestimated up to 70% for heavily sooting fuels when laser extinction measurements in the visible are interpreted using the Rayleigh scattering approximation, see Fig. 5.

2. The present scattering measurements in the large-angle regime yield aggregate fractal properties that are relatively independent of fuel type, as follows: fractal dimension, $D_f = 1.82$ with a standard deviation of 0.04; and fractal prefactor, $k_f = 8.1$ with a standard deviation of 0.09. These values agree within experimental uncertainties with earlier structure measurements for overfire soot (Köylü and Faeth, 1992a; Puri et al., 1992), and appear to be relatively robust properties of overfire soot aggregates.
3. Present scattering measurements in the large-angle regime at 514.5 nm yielded the soot refractive index ratio, $F(m)/E(m) = 0.74$ with a standard deviation of 0.09, over all the fuels. The refractive index measurements of Dalzell and Sarofim (1969) yield $F(m)/E(m) = 0.84$ which is in good agreement with present observations, while newer values from Tien and Lee (1981) and Chang and Charalampopoulos (1990) are somewhat higher, 1.55 and 1.10, respectively. The continued uncertainties of soot refractive indices are a substantial limitation to reliable nonintrusive laser-based measurements of soot properties and should be resolved.
4. The RDG polydisperse fractal aggregate theory provided reasonably good predictions of present soot optical property measurements. This was accomplished with predictions based solely on soot structure measurements in the large-angle regime, and after refitting the aggregate size distribution in the Guinier regime in order to adjust \bar{N}^2 that was not determined very accurately during the structure measurements. While this is promising, present measurements only approached the Guinier regime where potential deficiencies of the RDG scattering approximation should be most apparent. Thus, additional work at conditions where the Guinier regime is more dominant is needed in order to reliably establish the effectiveness of the RDG approximation for soot optical properties.

3. BUOYANT TURBULENT PLUMES

3.1 Introduction

This portion of the investigation involves the scalar mixing properties of round buoyant turbulent plumes in still environments. The mixing properties of plumes is an important fundamental problem that has attracted significant attention since the classical study of Rouse et al. (1952). However, recent work has highlighted the need for additional information concerning the turbulence properties of scalar quantities within buoyant turbulent flows, in order to address effects of turbulence/radiation interactions in fire environments, see Kounalakis et al. (1991) and references cited therein. In particular, the response of radiation to turbulent fluctuations largely is controlled by the moments, probability density functions, and temporal and spatial correlations of scalar property fluctuations. In turn, scalar property fluctuations largely can be represented by mixture fraction fluctuations using state relationships found from the laminar flamelet concepts, see Sivathanu and Faeth (1990b) and references cited therein. Thus, the overall objective of the present investigation was to complete measurements of mixture fraction fluctuation statistics. The study was limited to round buoyant turbulent plumes for several reasons: this fundamental configuration is important for benchmarking models of

buoyant turbulent flows, the results are directly relevant to the fuel-lean (overfire) region of fires, and considering a nonreactive environment is a logical first step toward studying mixture fraction fluctuations in the flaming portions of fires. In order to simplify interpretation of the results, the study emphasizes the properties of fully-developed buoyant turbulent plumes, where effects of the source have been lost and mean and turbulent quantities become self-preserving (Tennekes and Lumley, 1972).

The discussion of background from previous studies will be brief because several reviews of turbulent plumes have appeared recently (Kotsovinos, 1975; List, 1982; Papanicolaou and List, 1987). The earliest work concentrated on the scaling of flow properties within fully-developed turbulent plumes (Rouse et al., 1952; Morton, 1959; Morton et al., 1956). Measurements of mean properties within plumes generally have satisfied the resulting scaling relationships, however, there are considerable discrepancies among various determinations of centerline values, radial profiles and flow widths (Abraham, 1960; George et al., 1977; Kotsovinos, 1985; List, 1982; Rouse et al., 1952; Zimm and Frik, 1977). Aside from problems of experimental methods in some instances, List (1982) Papanicolaou and List (1987) attribute these discrepancies to problems of reaching fully-developed plume conditions.

Two parameters are helpful for assessing where fully-developed turbulent plume conditions are reached. The first of these is the distance from the virtual origin normalized by the source diameter, $(x-x_0)/d$. Based on results for nonbuoyant round turbulent jets, values of $(x-x_0)/d$ greater than ca. 40 and 100 are required for self-preserving profiles of mean and fluctuating properties, respectively (Tennekes and Lumley, 1972). By these measures, all past measurements involve transitional plumes, e.g., they generally are limited to $(x-x_0)/d < 40$, see Papanicolaou and List (1987) and references cited therein. The main reason for not reaching large values of $(x-x_0)/d$ for plumes similar to jets is that scalar properties decay at a much faster rate for plumes, e.g., proportional to $(x-x_0)^{-5/3}$ for plumes rather than $(x-x_0)^{-1}$ for jets, so that it is more difficult to maintain reasonable experimental accuracy far from the source within the plumes. A contributing factor is that plume velocities are relatively small in comparison to jets so that controlling room disturbances far from the source is much more difficult for plumes.

The second parameter useful for assessing conditions for fully-developed or self-preserving buoyant turbulent plumes is the distance from the virtual origin normalized by the Morton length scale, $(x-x_0)/\ell_M$. The Morton length scale is defined as follows for a round plume (Morton, 1959; List, 1982):

$$\ell_M = (\rho_\infty u_0^2 / (g|\rho_0 - \rho_\infty|))^{1/2} \quad (30)$$

where an absolute value has been used for the density difference in order to account for both rising and falling plumes. Thus, large $(x-x_0)/\ell_M$ represents the distance required for buoyancy-induced momentum to become large in comparison to the source momentum so that buoyant features of the flow are dominant. The ratio of the two normalizing factors, ℓ_M and d , is the source Froude number, defined as follows:

$$Fr_0 = \ell_M/d = (\rho_\infty u_0^2 / (g|\rho_0 - \rho_\infty|d))^{1/2} \quad (31)$$

which quantifies the initial degree of buoyant behavior of the source, e.g., $Fr_0 = 0$ for a purely buoyant source. Papanicolaou and List (1987) suggest that buoyancy-dominated conditions for mean and fluctuating quantities are reached for $(x-x_0)/\lambda_M$ greater than ca. 6 and 14, respectively. A greater proportion of existing data for mean properties exceed this criterion, however, the effect of transitional plume behavior (in terms of $(x-x_0)/d$) on the observations of Papanicolaou and List (1987) is uncertain, as is the degree of buoyancy dominance for existing plume measurements.

Naturally, in instances where reaching self-preserving conditions for mean properties is questionable, it is likely that turbulence properties are transitional. Thus, the measurements of George et al. (1977) of plume streamwise velocity and temperature intensities and probability density functions, and correlations of velocity and temperature fluctuations, where x/d is in the range 8-16, clearly do not represent self-preserving conditions. Similarly, measurements of Papanicolaou and List (1987) of temperature intensities and probability density functions of thermal plumes for x/d in the range 12.5-20 represent transitional conditions as well. Additionally, Papanicolaou and List (1987) measure the power spectra of temperature fluctuations at a greater distance, $x/d = 53$, however, this condition only involved $x/\lambda_M = 1.52$ so that it is unlikely that buoyancy-dominated conditions were achieved. Other properties of interest for simulations of turbulence/radiation interactions — spatial correlations and spatial and temporal integral scales — have not been measured at all. Thus, existing results concerning the turbulence properties of plumes are rather limited and do not address the self-preserving plume region.

The preceding discussion has indicated that existing measurements of mean and fluctuating properties within plumes involve transitional plumes that are evolving toward fully-developed turbulent plume conditions from generally poorly defined source conditions. In addition, available results for turbulence properties do not include crucial information required to interpret effects of turbulence/radiation interactions (Kounalakis et al., 1991). Thus, the objective of the present investigation was to complete measurements of the mean and fluctuating mixture fraction properties of buoyant turbulent plumes, emphasizing conditions within the fully-developed turbulent plume region. The mixture fraction properties considered included mean and fluctuating values, probability density functions, temporal power spectra, radial spatial correlations, and temporal and spatial integral scales. The experiments involved source flows of carbon dioxide and sulfur hexafluoride in still air at atmospheric pressure and temperature. This yielded downward flowing negatively-buoyant plumes. Measurements of mixture fractions were undertaken using laser-induced iodine fluorescence (LIF).

3.2 Experimental Methods

Test Apparatus. A sketch of the experimental apparatus appears in Fig. 6. In order to control room disturbances or contamination of adjacent areas with iodine vapor, the plumes were observed in a double enclosure contained within a large, high-bay test area. The outer enclosure ($3000 \times 3000 \times 3400$ mm high) had plastic side walls with a screen across the top for air inflow in order to compensate for air entrained by the plume. The plume itself was within a smaller enclosure ($1100 \times 1100 \times 3200$ mm high) with plastic screen walls (630 wires/m with a wire diameter of 0.25 mm). The smaller enclosure was mounted on linear bearings and could be traversed in one direction using a

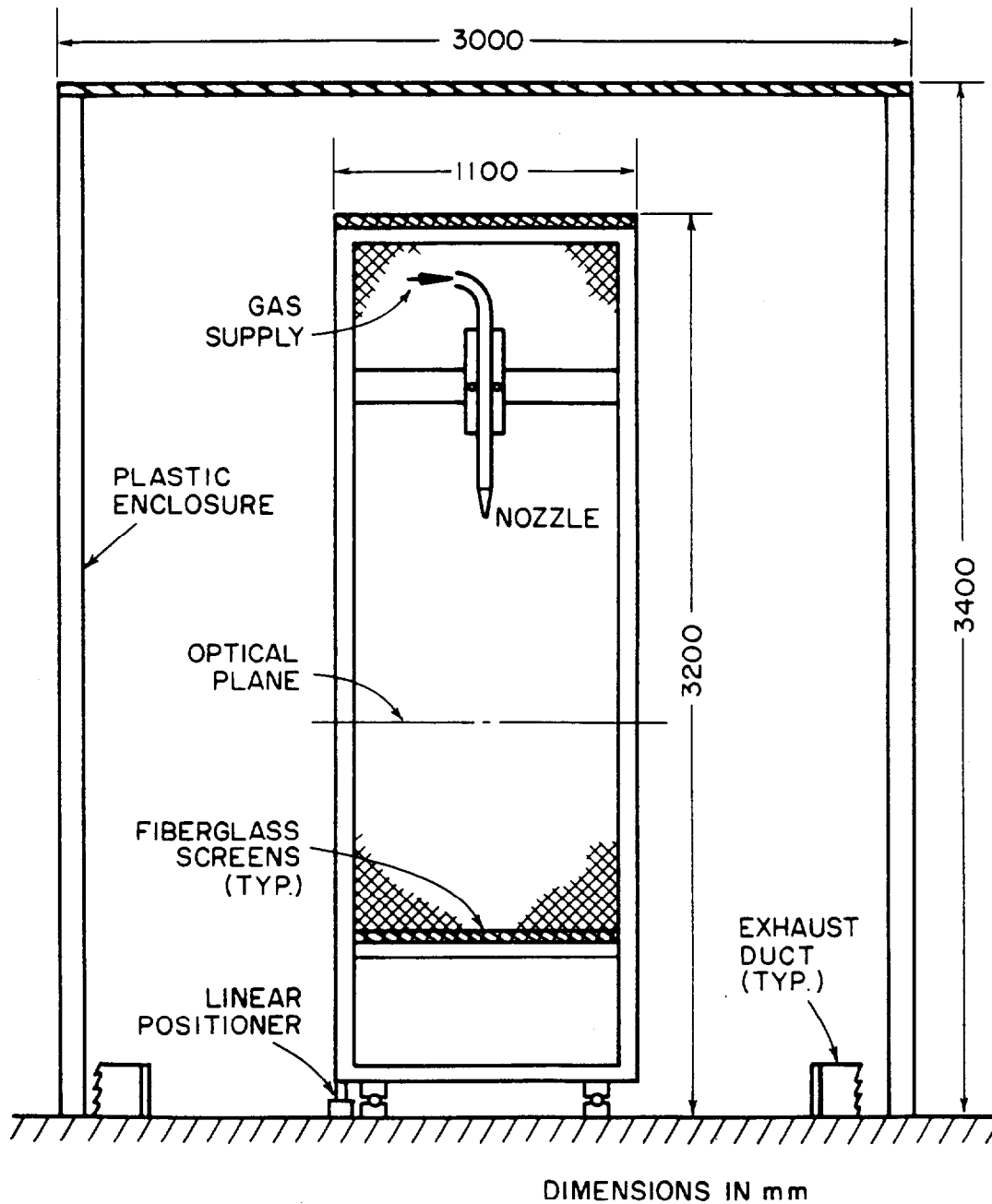


Figure 6. Sketch of the buoyant turbulent plume apparatus

stepping motor driven linear positioner (5 μm positioning accuracy) in order to accommodate rigidly mounted instrumentation. The plume flow was removed through 300 mm diameter ducts located at the four corners of the outer enclosure. The exhaust flow was controlled by a bypass/damper system in order to match plume entrainment rates and minimize flow disturbances. All components that might contact iodine vapor were either plastic or painted, or were sealed in plastic wrap, in order to prevent corrosion. The outer plastic enclosure satisfactorily prevented iodine contamination of adjacent areas.

The plume source consisted of rigid plastic tubes having inside diameters of 6.4 and 9.7 mm with flow straighteners at the inlet. The tubes had length-to-diameter ratios of 50:1 to yield fully developed turbulent pipe flow at the exit since source Reynolds numbers were greater than 2000. The outside surface of the tubing exit was chamfered at an angle of 30° to reduce the separation disturbances of the plume-entrained flow. The source could be traversed in the vertical direction (0.25 mm positioning accuracy) to accommodate measurements at different streamwise positions.

The source flows were either carbon dioxide or sulfur hexafluoride. The carbon dioxide and sulfur hexafluoride were stored under pressure in commercial cylinders. Gas flow rates were controlled and measured using pressure regulators in conjunction with critical flow orifices. All flow rates were calibrated using wet test meters. After metering, mixing and addition of iodine vapor, the flow passed through a flexible plastic tube having a length-to-diameter ratio of 800 in order to insure a uniform composition at the source exit.

The flow was seeded with iodine vapor by passing a portion of it through a bed of iodine crystals (bed diameter and depth of 100×200 mm). The bed operated at room temperature and the flow was saturated with iodine at the exit of the bed; therefore, the concentration of iodine vapor varied with changes of room temperature, so that the LIF signal was monitored with the fraction of flow entering the iodine bed periodically adjusted to control signal levels. The iodine crystals were reagent grade, with initial flake shapes having diameters of 2-8 mm and thicknesses of 0.5 mm.

Instrumentation. Mixture fractions were measured using iodine LIF, similar to earlier studies of wall plumes in this laboratory (Lai and Faeth, 1987a,b; Lai et al., 1986). A sketch of the arrangement appears in Fig. 7. The LIF signal was produced by the unfocused beam (beam diameter at the e^{-2} points of 1.5 mm) of an Argon-ion laser having an optical power of roughly 1800 mW at the green 514.5 nm line. This wavelength is absorbed by iodine and causes it to fluoresce at longer wavelengths in the visible yellow portion of the spectrum (Hiller and Hanson, 1990). The laser beam was horizontal and crossed through the plume axis at roughly 1500 mm above the floor of the enclosure. The operation of the laser beam was monitored with two laser power meters (Newport, Model 820): one measuring laser power before crossing the flow to detect laser power variations, the other measuring laser power after passing through the flow in order to correct the laser beam power at the measuring locations for absorption by iodine vapor.

The fluorescence signals were measured using two-detectors, one mounted rigidly and the other traversible along the laser beam to provide measurements of two-point spatial correlations in the radial direction. Since the plume source could be traversed horizontally and vertically, all points in the flow could be addressed for two-point measurements. The fluorescence signals were observed at right angles to the laser beam with f2 collecting lenses having diameters of 80 mm. The apertures of the detectors

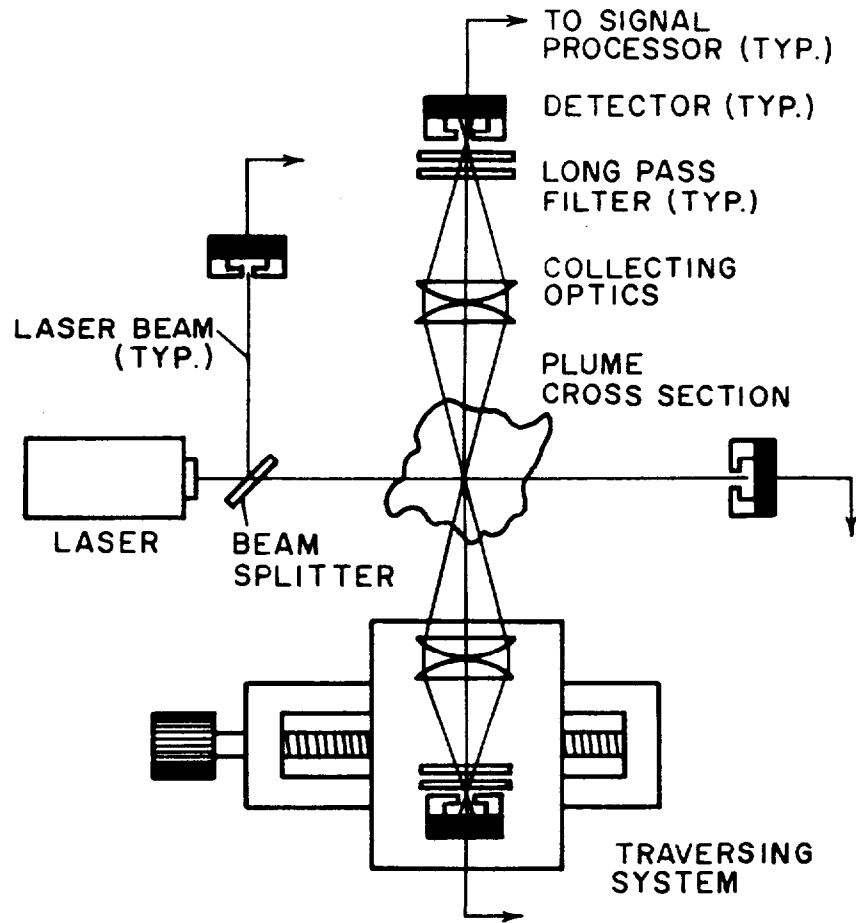


Figure 7. Sketch of the two-point LIF system

(Hamamatsu R268) were selected to give measuring volumes having diameters of 1 mm with lengths of 1.5 mm set by the laser beam diameter. The LIF signal was separated from light scattered at the laser line using long-pass optical filters (cut-off wavelengths of 520 nm). The detector outputs were amplified and then low-pass filtered to control alias signals using Ithaco, Model 4213 electronic filters (sixth-order Chebychev filters) with break frequencies of 500 Hz. The signals then were sampled using an a/d converter and buffer storage system (LeCroy, Models 8800, 82/2A/8, 8901A). The digital output was transferred to an IBM-AT clone computer for processing and storage. The detector signals also were monitored using a LeCroy Model 9400 A digital oscilloscope.

Both the absorption and LIF signals were calibrated by measurements across the source exit, by mixing the source flow with air to vary the mixture fraction, analogous to the plume flow. These tests showed that fluctuations of iodine seeding levels were small, less than 1%. The LIF signal was not saturated for present conditions and varied linearly with laser power. The LIF signal also varied linearly with the number of iodine molecules present per unit volume, i.e., with the partial density of iodine, while reabsorption of scattered light was small (less than 10%). Thus, the relationship between the LIF signal level and the mixture fraction for signal processing was obtained from the state relationship for an ideal gas mixture. This relationship was nearly linear for the carbon dioxide source flow due to modest density variations but had significant nonlinearities for the sulfur hexafluoride source flow where the density variation was substantial. These calibrations were checked periodically by diverting the source flow through a plastic tube whose exit was mounted temporarily just above the measurement locations. Final processing of the signals accounted for absorption of the laser beam by iodine vapor and laser beam power variations.

Gradient broadening errors were negligible (less than 1%) at the locations where measurements were made. Thus, signal sampling times were controlled to maintain experimental uncertainties (95% confidence) along the axis less than 5% for mean mixture fractions and 10% for mixture fraction fluctuations, both being repeatable well within these ranges. These uncertainties were maintained up to $r/(x-x_0) = 0.15$ but increased at larger radial distances, roughly inversely proportional to f .

Test Conditions. The test conditions for the buoyant turbulent plume experiments are summarized in Table 5. Two flows were considered, involving a carbon dioxide and sulfur hexafluoride, the latter allowing measurements at greater values of $(x-x_0)/d$ and $(x-x_0)/Q_M$ due to its smaller source diameter and faster rate of development. Initial velocities at the source exit were chosen to yield Reynolds numbers for turbulent pipe flow at the source exit, in order to enhance rates of development toward fully-developed turbulent plume conditions. Nevertheless, the carbon dioxide flow was marginally turbulent with the virtual origin displaced a substantial distance from the source exit. The source Froude numbers were comparable to current estimates of asymptotic Froude numbers in order to enhance development of the buoyant properties of the flow. Nevertheless, the Morton length scales were significantly larger than the source diameter with Q_M/d of 7.34 and 3.53 for the carbon dioxide and sulfur hexafluoride flows, respectively.

The measurements involved mean and fluctuating mixture fraction properties at various streamwise positions. Mean properties were then scaled in terms of the self preserving variables of fully-developed turbulent plumes, as follows (List, 1982):

$$\bar{f} = (\pi Fr_0/4)^{2/3} (\rho_0/\rho_\infty) ((x-x_0)/d)^{-5/3} F(r/(x-x_0)) \quad (32)$$

Table 5. Buoyant Turbulent Plume Test Conditions^a

Source Properties	Carbon Dioxide	Sulfur Hexafluoride
Density (kg/m ³)	1.75	5.87
Kinematic viscosity (mm ² /s)	8.5	2.6
Diameter (mm), d	9.7	6.4
Average velocity (m/s), u_0	1.74	1.89
Reynolds number, $u_0 d / \nu_0$	2,000	4,600
Froude number, equation (31)	7.80	3.75
Morton length scale, ℓ_M / d	7.34	3.53
Virtual origin, x_0 / d	12.7	0.0
Maximum $(x - x_0) / d$	111.2	151.0
Maximum $(x - x_0) / \ell_M$	15.2	42.6

^aFlow directed vertically downward in still air with ambient pressure and temperature of 99 ± 0.5 k Pa and 297 ± 0.5 K. Source length-to-diameter ratios of 50:1.

where $F(r/(x-x_0))$ represents the appropriately scaled radial profile function of mean mixture fractions. This equation then was used to extrapolate measurements of mean mixture fractions along the axis in order to identify the vertical origin that yielded the best fit of the data. As noted earlier, the location of the virtual origin is controlled by source properties like turbulence levels and initial Froude numbers, however, it was beyond the scope of the present investigation to quantitatively study these relationships. The resulting streamwise ranges of the measurements are summarized in Table 5, notably they extend up to $(x-x_0)/d = 151.0$ and $(x-x_0)/\mathcal{L}_M = 42.6$, which exceed existing measurements by a wide margin and provide results well within the self-preserving region of buoyant turbulent plumes.

3.3 Results and Discussion

Mean Properties. The variation of mean mixture fractions along the axis of the carbon dioxide plume are illustrated in Fig. 8. In this case, density variations throughout the flow are modest so the results can be illustrated directly without variable-density scaling. In addition, correlations proposed by Rouse et al. (1952) and George et al. (1977) for fully developed plumes are shown on the plot. Present measurements suggest transitional behavior up to $(x-x_0)/d$ ca. 40, beyond which \bar{f} becomes proportional to $(x-x_0)^{-5/3}$ which is the variation anticipated from equation (32). Thus, it is likely that earlier results, such as the measurements of George et al. (1977), represent transitional plume conditions even though they could be scaled according to equation (31) over the available narrow range of streamwise distances where fully-developed turbulent plume behavior was approached. The early measurements of Rouse et al. (1952) present a different problem because the source was a flame so that source diameters and Morton length scales are difficult to define, however, subsequent results suggest that these plumes were transitional as well.

A more detailed picture of the development of transitional plumes toward fully-developed conditions can be obtained from the radial profiles of mean mixture fractions for the carbon dioxide/air plumes illustrated in Fig. 9. In this case, the scaling parameters of equation (32) are used for results at various streamwise distances. The radial correlations of mean mixtures fractions from Rouse et al. (1952) and George et al. (1977) also are shown on the plot; these have the following forms, respectively:

$$F(r/(x-x_0)) = 11.0 \exp (-71(r/(x-x_0))^2) \quad (33)$$

$$F(r/(x-x_0)) = 9.1 \exp (-65(r/(x-x_0))^2) \quad (34)$$

Examining the evolution of the present measurements with streamwise distance it is evident that the profiles only become self-preserving for $(x-x_0)/d$ larger than ca 40, and that the scaled mixture fraction profiles in the fully-developed region are larger at the axis and narrower than those of Rouse et al. (1952) and George et al. (1977).

Measurements of radial profiles of mean mixture fractions in the fully-developed turbulent plume region are illustrated in Fig. 10. In this case results at the two largest distances from the source for the carbon dioxide plumes are shown along with results for $25.0 \leq (x-x_0)/d \leq 151.0$ for the sulfur hexafluoride plumes. All these results involve $(x-x_0)/\mathcal{L}_M > 7.0$ so that buoyancy properties of the flow should be reasonably well developed. The measurements yield the same self-preserving profiles within experimental uncertainties, notwithstanding nearly an order of magnitude increase of $(x-x_0)/d$ for the sulfur hexafluoride plumes. As noted earlier, the profiles of Rouse et al. (1952) and George et al. (1977), also shown on the plot, are wider and have smaller centerline

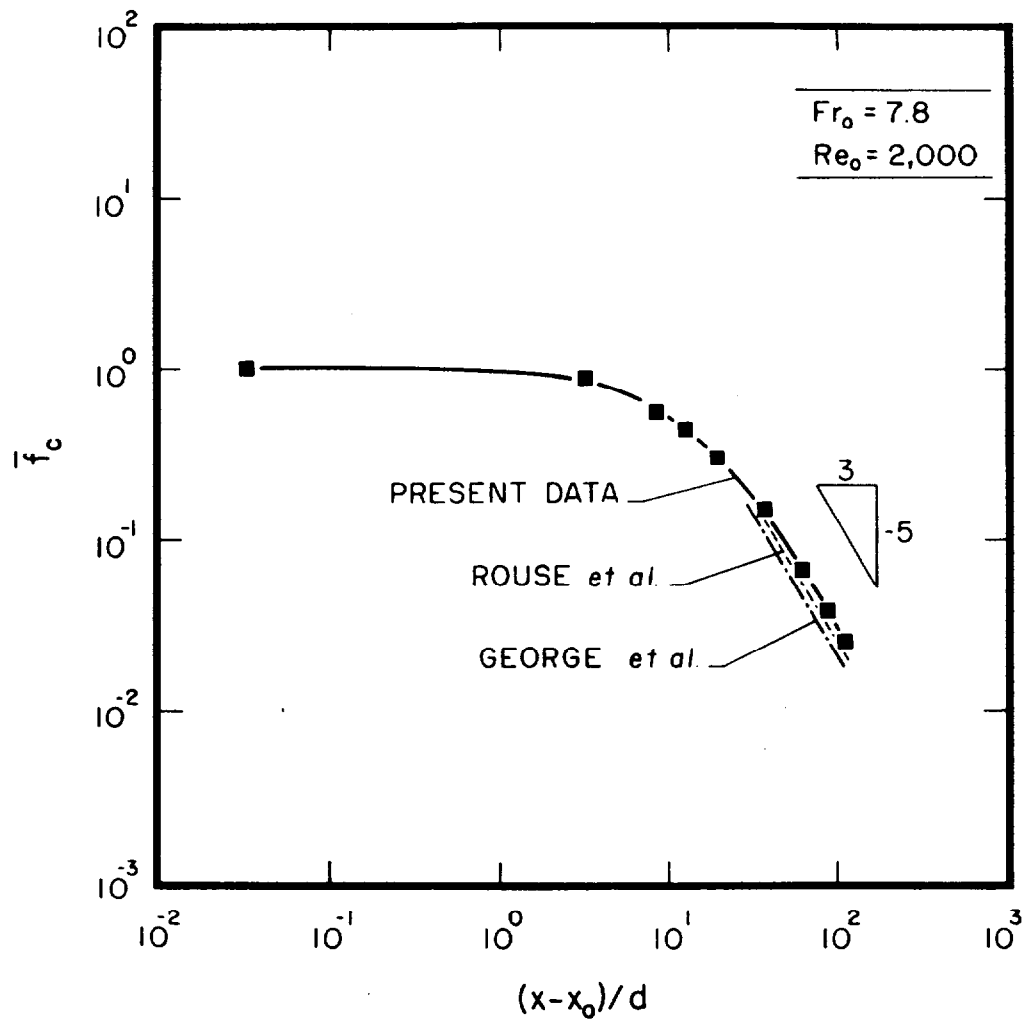


Figure 8. Mean mixture fractions along the plume axis

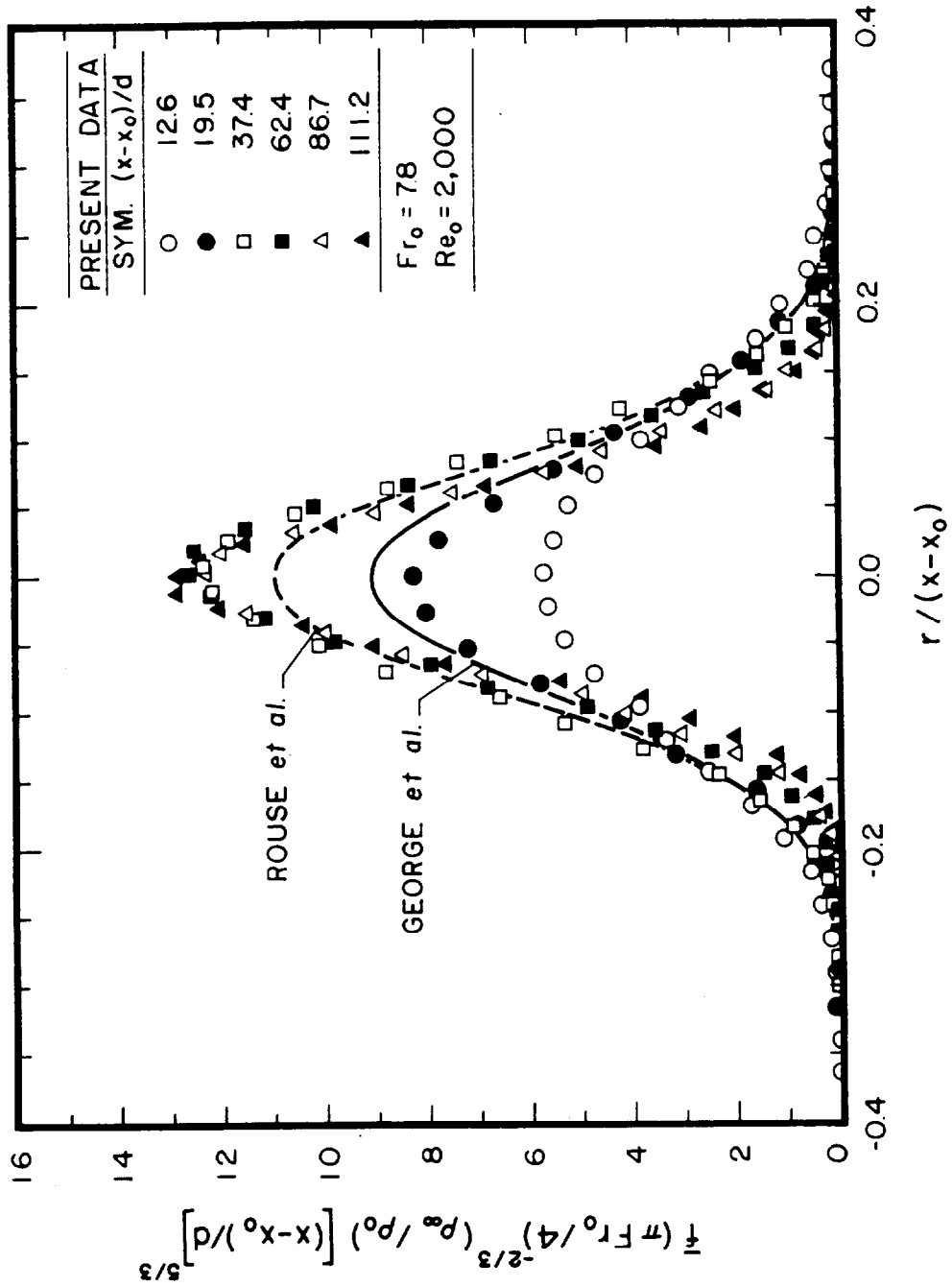


Figure 9. Development of radial profiles of mean mixture fractions

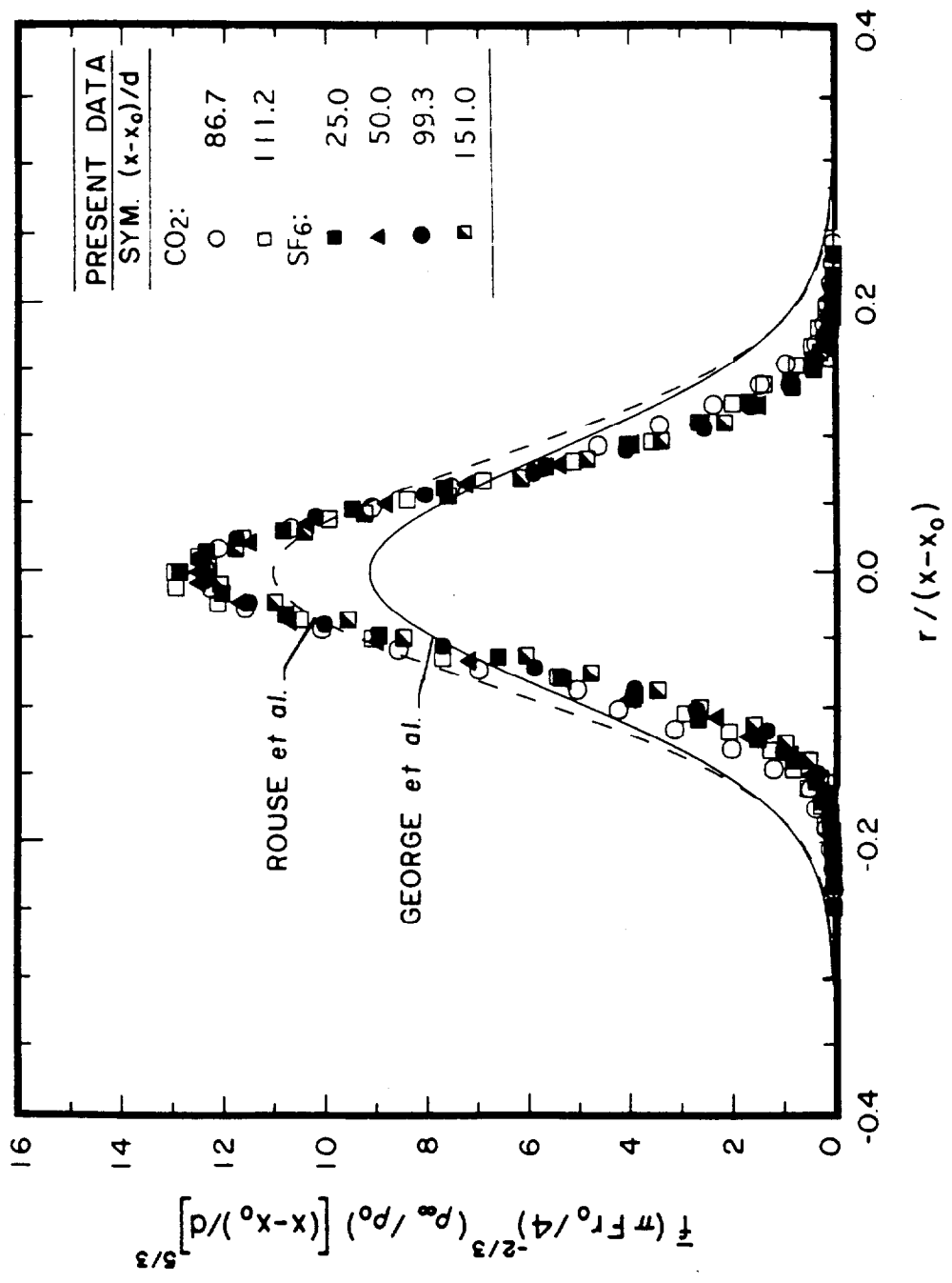


Figure 10. Radial profiles of mean mixture fractions in the fully-developed turbulent buoyant plume region

values. However, more recent results of Papanicolaou and List (1987), which extend up to $(x-x_0)/d$ of 40, are correlated in terms of centerline values as follows:

$$\bar{f}/\bar{f}_c = \exp(-80(r/(x-x_0))^2) \quad (35)$$

taking mixture fraction to be proportional to the normalized temperature variation of their flow, which is reasonable in view of the modest temperature variations involved. Equation (35) fits the present measurements in the fully-developed plume region, within experimental uncertainties, when they are plotted in this manner. Thus, it appears that existing results in the self-preserving region for mean properties, are reasonably consistent, with $(x-x_0)/d$ of ca. 40 providing a reasonable estimate of the onset of this region.

Turbulence Properties. Radial profiles of mixture fraction fluctuations at various distances from the source for the carbon dioxide/air plumes are plotted in Fig. 11. Correlations of the measurements of George et al. (1977) and Papanicolaou and List (1987) also are shown on the plot (the latter being incorrectly denoted List et al.). The present results show a clear evolution of the profiles from results near the source, where fluctuations dip toward the axis somewhat like nonbuoyant jets, to eventually attain nearly self-preserving behavior for $(x-x_0)/d \geq 86.7$. Results for the sulfur hexafluoride plumes were similar, with self-preserving conditions reached within experimental uncertainties for $(x-x_0)/d \geq 99.3$. This behavior is typical of other turbulent jet and wake flows where the streamwise development for turbulence quantities is slower than for mean quantities, and generally twice the streamwise distance is required for self-preserving turbulence properties in comparison to mean properties. Thus, the measurements of George et al. (1977) and Papanicolaou and List (1987) for $(x-x_0)/d$ less than 40 are representative of transitional plumes with respect to turbulence properties.

The gradual disappearance of the dip in mixture fraction fluctuations is an interesting feature of the results illustrated in Fig. 11. The development of the flow from source conditions, where mixture fraction fluctuations are small, less than 1%, is certainly a factor in this behavior. However, the gradual disappearance of nonbuoyant dynamics as $(x-x_0)/L_M$ becomes large probably also plays a role in this behavior. In particular, nonbuoyant jets have reduced mixture fraction fluctuations near the axis because turbulence production is small in this region in view of symmetry requirements (Becker et al., 1967; Papanicolaou and List, 1987). In contrast, effects of buoyancy provide turbulence production near the axis for plumes in spite of symmetry due to buoyant instability in the streamwise direction, i.e., the density approaches the ambient density in the streamwise direction. This added turbulence production accounts for increased mixture fraction fluctuation levels near the axis of plumes than jets in the self-preserving region, i.e., $(\bar{f}'/\bar{f})_c$ ca. 0.45 for plumes in comparison to 0.15-0.18 for jets (Papanicolaou and List, 1987). Even maximum values of \bar{f}'/\bar{f}_c in jets are substantially less than the maximum plume values, ca. 0.25 at an $r/(x-x_0)$ of roughly 0.1 (Papanicolaou and List, 1987). Thus, the contribution of buoyancy to turbulence is appreciable, with the large mixture fraction fluctuations of turbulent plumes helping to explain the large radiation fluctuation levels observed in the near-overfire region of buoyant turbulent diffusion flames (Kounalakis et al., 1991).

Mean and fluctuating velocities are reasonably descriptive because the probability density functions of velocities in turbulent flows generally are well represented by a Gaussian distribution function that only has two moments. This not the case for the probability density functions of mixture fraction, however, because the mixture fraction is limited to the finite range 0-1 by definition and intrinsically can not have a Gaussian probability density function. Thus, finite range distribution functions must be used, e.g.,

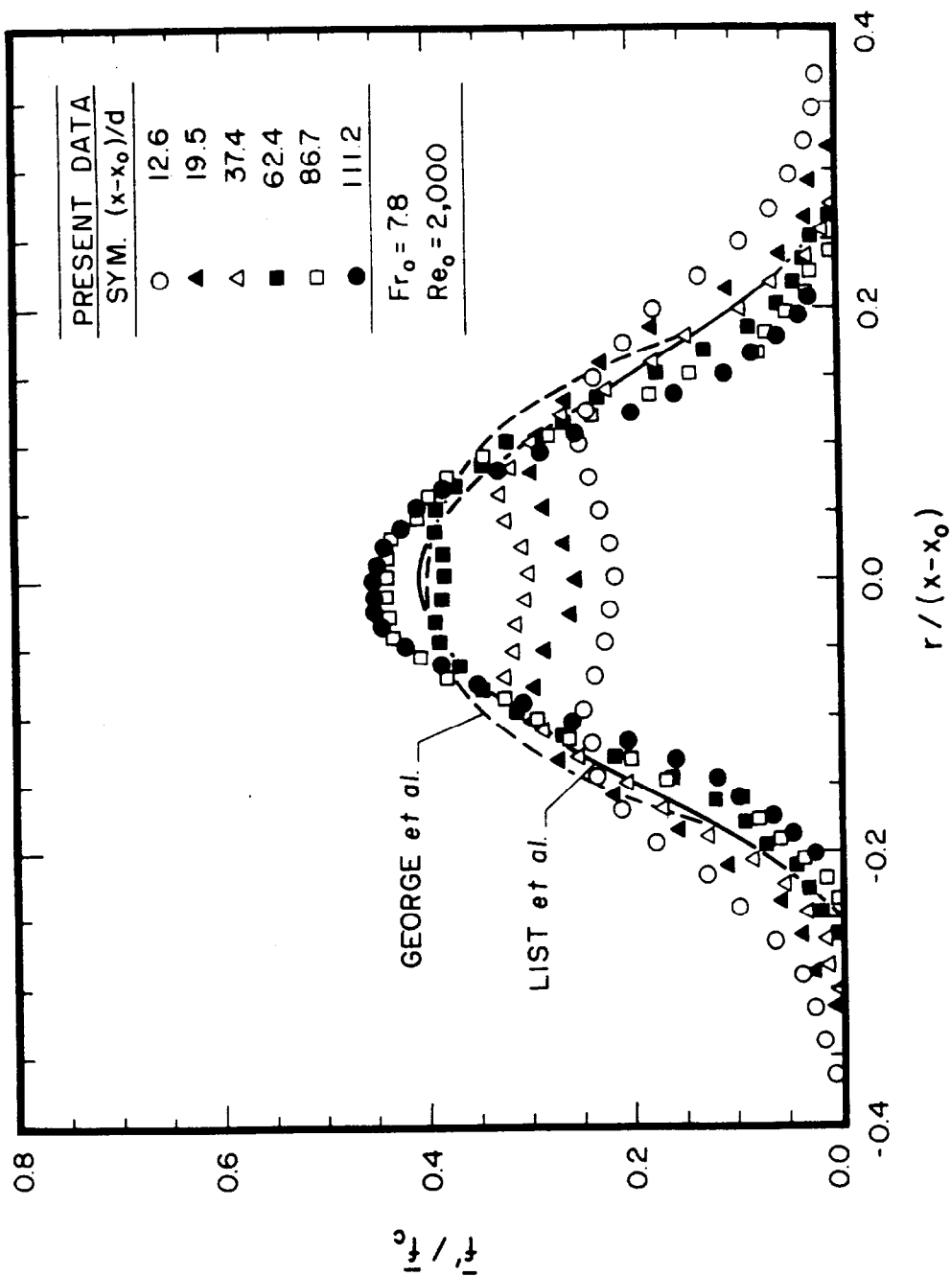


Figure 11. Radial profiles of mixture fraction fluctuations

the clipped-Gaussian function that has been used for simulations to find turbulence/radiation interactions (Kounalakis et al., 1991) or the algebraically more convenient beta function. Thus, some typical probability density functions from present measurements are plotted along with these distributions in Fig. 12. Both distributions are defined by two moments, thus, the predicated distributions are based on the measured values of f and f' at each location considered.

The measured probability density functions illustrated in Fig. 12 are qualitatively similar to earlier measurements for flames, plumes and jets (Kounalakis et al., 1991; Lai and Faeth, 1987b; Papanicolaou and List, 1987; Becker et al., 1967). Near the axis, the probability density function is nearly Gaussian, although it still has a small spike at $f = 0$ representing some periods when unmixed ambient fluid reaches the axis. With increasing radial distance, the spike at $f = 0$ increases and eventually dominates the distribution as the edge of the plume is approached. There is little to choose between representing the probability density functions by either clipped-Gaussian or beta functions, although the ease of use of the beta function in simulations is helpful for reducing computation times.

Temporal correlations, or temporal power spectral densities, of mixture fraction fluctuations must be known to simulate the temporal aspects of radiation fluctuations (Kounalakis et al., 1991); these properties also are valuable for gaining an understanding of turbulent mixing (Tennekes and Lumley, 1972). Some typical measurements of temporal power spectra for the carbon monoxide plumes are illustrated in Fig. 13. Results along the axis are shown on the plot, extending up to $(x-x_0)/d = 86.7$ where the turbulence properties become self-preserving, with the radial variation of the spectra illustrated at this position as well. The temporal spectra are seen to be a rather robust property of the turbulence, with results normalized by τ and f' being identical over the range shown in the figure, including results at $(x-x_0)/d = 12.6$ where the turbulence is not very well developed (cf. Fig. 11). Thus, the measurements of temporal spectra of transitional plumes by Papanicolaou and List (1987) are qualitatively quite similar to the results illustrated in Fig. 13.

The decay of the spectra with increasing frequency is an interesting feature of the results illustrated in Fig. 13. The spectra initially decay according to the $-5/3$ power of frequency. This initial decay region is analogous to the well known inertial region of the turbulence spectrum of velocity fluctuations, and has been called the inertial-convective region for scalar property fluctuations (Tennekes and Lumley, 1972). Within this region, mixture fraction fluctuations simply are convected and effects of molecular diffusivities are small. This is followed by a region where the spectrum decays more rapidly, yielding a slope of roughly -3 , that has been observed during several investigations of highly buoyant flows with molecular Prandtl/Schmidt numbers in the range 0.7-7, but not in nonbuoyant flows (Mizushima et al, 1979; Papanicolaou and List, 1987). Papanicolaou and List (1987) argue that this portion of the spectrum is in accord with behavior expected for the inertial-diffusive subrange, where the variation of the local rate of dissipation of mixture fraction fluctuations in buoyant flows is due to buoyancy-generated inertia forces rather than viscous forces. However, understanding of the behavior of the spectra of buoyant turbulent flows in this region is very limited and clearly merits additional study since several studies have confirmed the -3 inertial-diffusive region for fluids whose Prandtl/Schmidt numbers are not unusually small. At higher frequencies, the mixture fraction microscale should be approached where the spectrum becomes small; unfortunately, existing measurements, including the present study, have not had spatial or temporal resolutions needed to resolve this region.

The definitions of temporal correlations and spectra are completed by the temporal integral scale which is plotted for present carbon monoxide/air plumes in Fig.

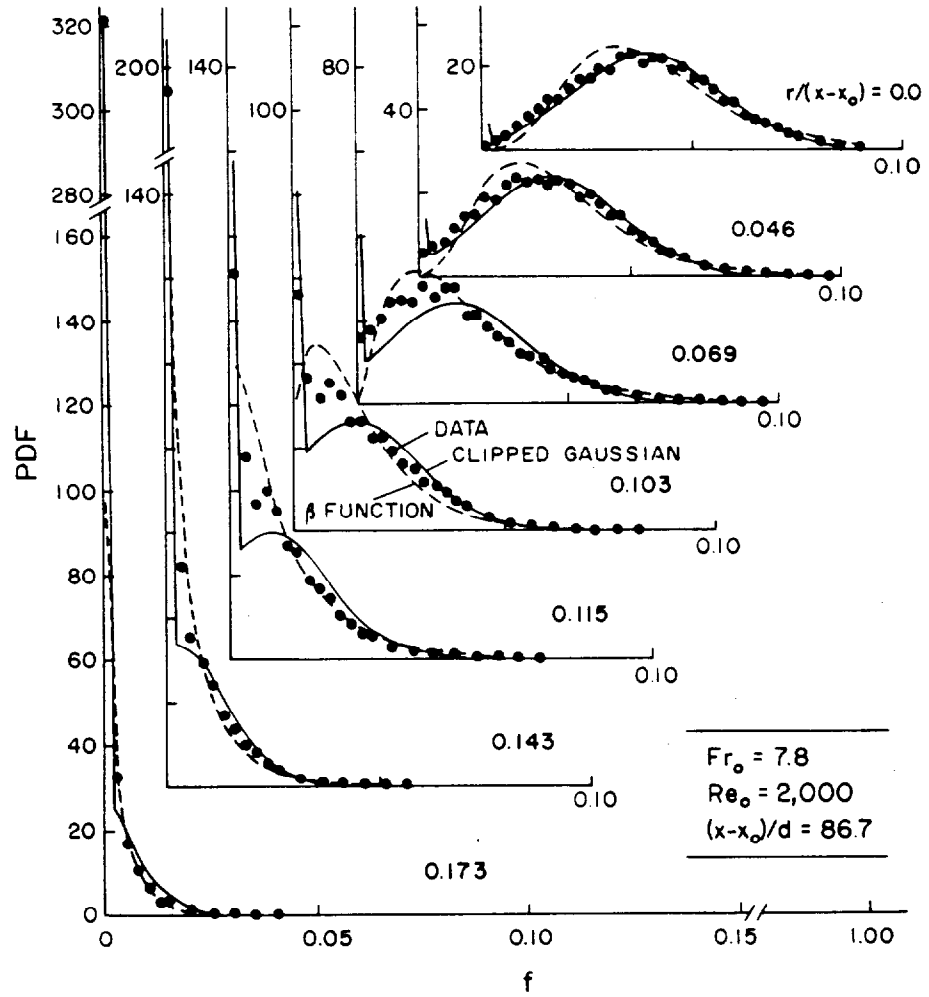


Figure 12. Probability density functions of mixture fractions at $(x-x_0)/d = 86.7$

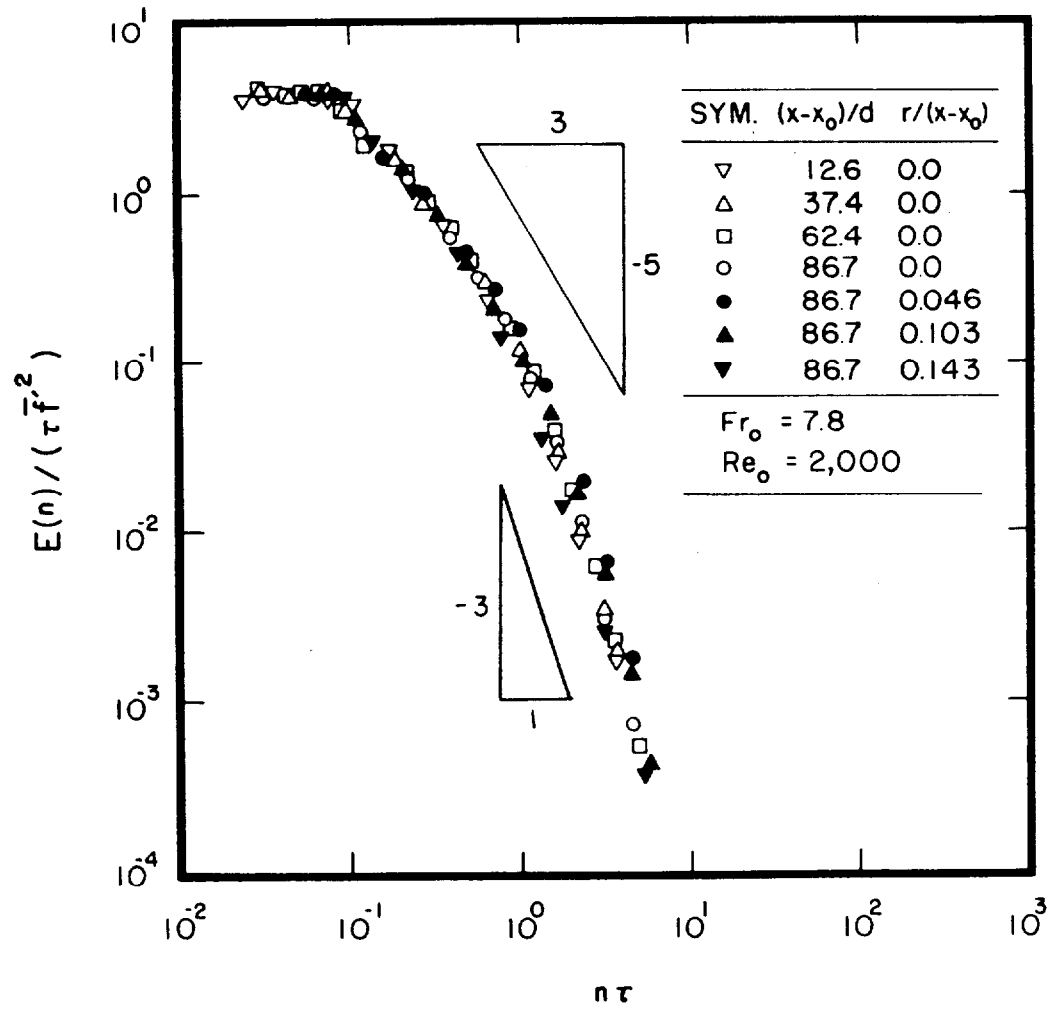


Figure 13. Temporal power spectral densities of mixture fraction fluctuations

14. These results have been plotted by adopting Taylor's hypothesis for the relationship between spatial and temporal integral scales, and using fully-developed turbulent plume scaling relationships for integral length scales and mean velocities, i.e., that length scales vary linearly with $(x-x_0)$. This approach appears to provide a reasonable correlation of the data at the two streamwise positions shown, although further study of this scaling is needed using all the measurements available from the data. The results show a progressive increase of τ with radial distance over the test range. This follows from Taylor's hypothesis, noting that spatial integral scales are relatively independent of radial distance (which will be shown later) while streamwise mean velocities decrease as the edge of the flow is approached.

The general properties of spatial correlations in turbulent shear flows vary depending on whether the two points considered are on the same or opposite sides of planes or lines of symmetry. This orientation will be indicated by a coordinate system along the radial direction extending from $-\infty$ to ∞ with Δr always greater than zero and the left-most position denoting the position of the correlation. Thus, $r < 0$ implies that both points are on the same side of the axis for $\Delta r < |r|$ and on opposite side thereafter. If $r > 0$, then both points always are on the same side of the axis. Finally, Corrsin and Uberoi (1950) introduced symmetric lateral spatial correlations for jets, where the two points are spaced equally on either side of the axis (at $-\Delta r/2$ and $\Delta r/2$); thus, there is only one correlation of this type at each streamwise position.

Present measurements of positive and symmetric radial spatial correlations are plotted in Fig. 15, along with measurements of symmetric spatial correlations due to Becker et al. (1967) and Corrsin and Uberoi (1950) for round jets. Present measurements are for carbon dioxide plumes in the self-preserving region for turbulence quantities. The positive correlations exhibit an exponential decay, similar to the observations in flames of Kounalakis et al. (1991). This behavior is an artifact of experimental limitations: the region near $\Delta r = 0$ should have a nonexponential (quadratic) behavior as the microscale limit is approached (Becker et al., 1967). This is not seen in the present measurements because the spatial resolution was not adequate to resolve the smallest scales. All the symmetric spatial correlations have a Frenkiel function shape with a maximum negative value in the range -0.1 to -0.2 for $\Delta r/(x-x_0)$ in the range 0.10 - 0.15 . It is likely that this behavior follows from a conservation of scalar flux requirement, where fluctuations of one sign must be compensated by fluctuations of the other sign on the opposite sides of the axis so that the mixture fraction flux is preserved as a whole. Similar behavior is well known for the lateral spatial correlations of velocity fluctuations in isotropic turbulence due to conservation of mass requirements (Hinze, 1975). Present measurements in plumes reach smaller negative values than the jets, however, due to limited available data it is difficult to know whether this is an effect of buoyancy or just a measure of experimental uncertainties. In any event, interpreting the Frenkiel function shape of the symmetric correlations will require consideration of velocities (or scalar fluxes) because the mixture fraction flux depends on both the velocity and mixture fraction fields.

The measured spatial correlations for negative r are plotted in Fig. 16 for the carbon dioxide plumes in the self-preserving region for turbulence quantities. Fits of the positive and symmetric correlations for plumes also are shown on the plots. The correlations for $r < 0$ are seen to be bounded by the positive and symmetric correlations which is a natural consequence of the position of the points. For example, when $\Delta r < |r|$ both points are on the same side of the axis and should correspond to the positive correlations. On the other hand, when $\Delta r = 2|r|$ for $r < 0$, the symmetric correlation condition is retrieved. Not surprisingly, other positions exhibit intermediate behavior. As noted earlier, the behavior of these correlation involves scalar flux considerations and

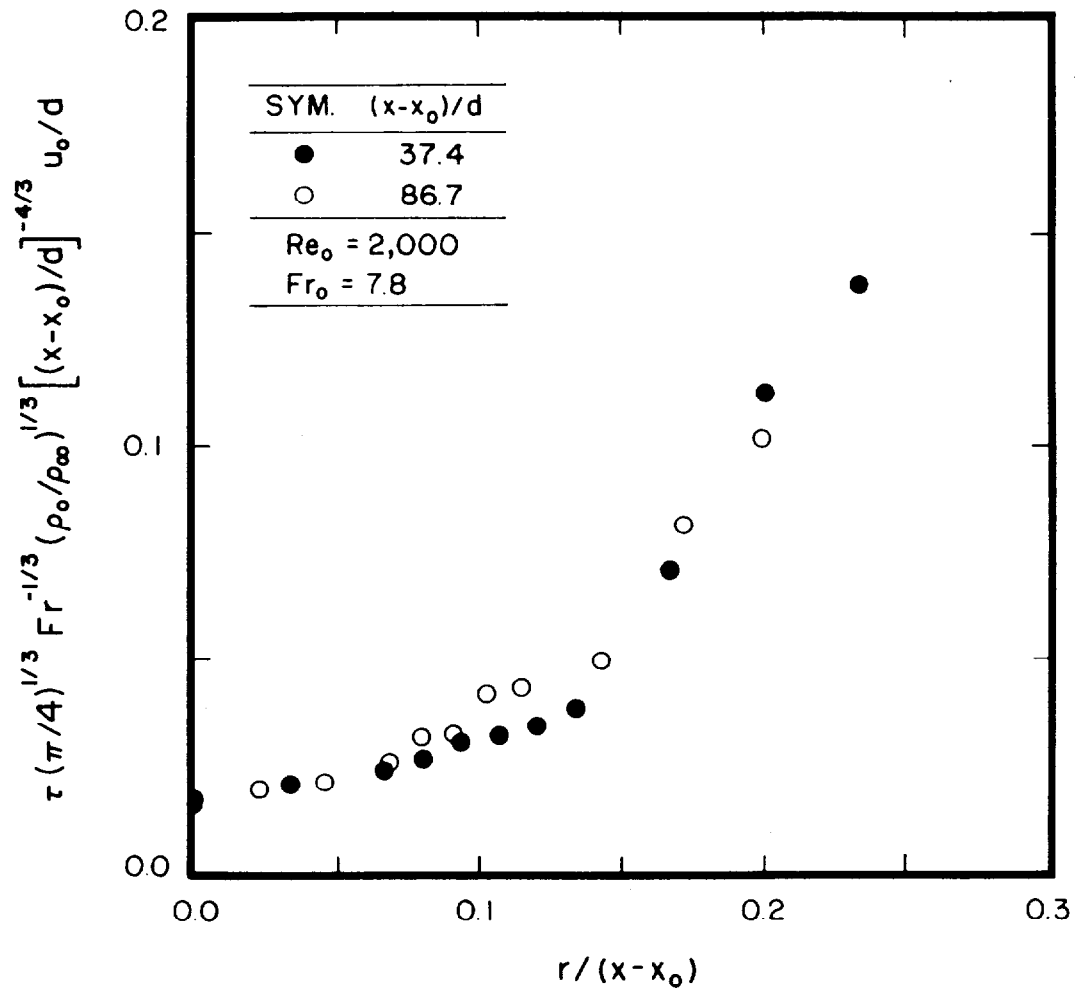


Figure 14. Radial profiles of temporal integral scales

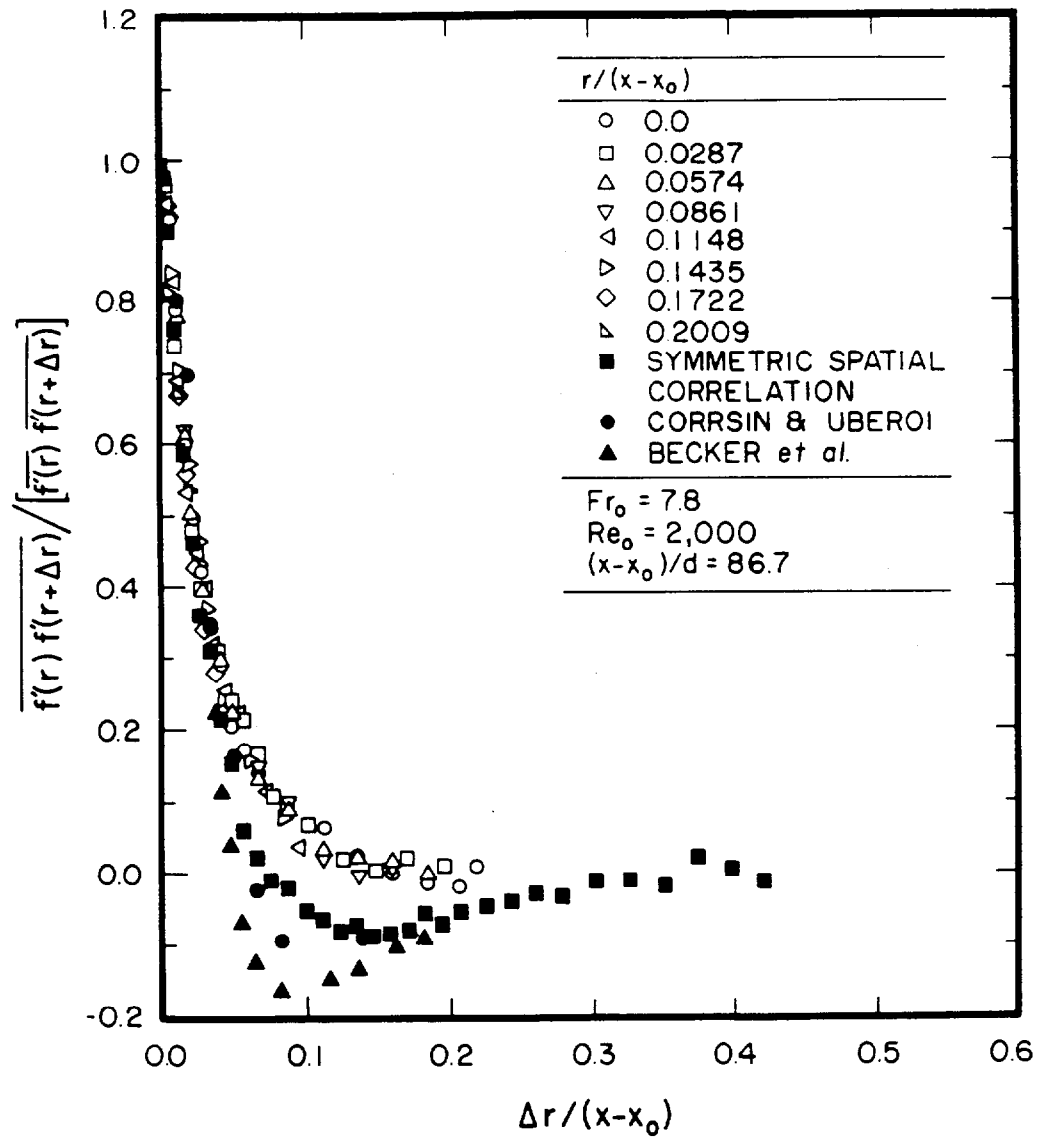


Figure 15. Symmetric and positive spatial correlations of mixture Fraction fluctuations

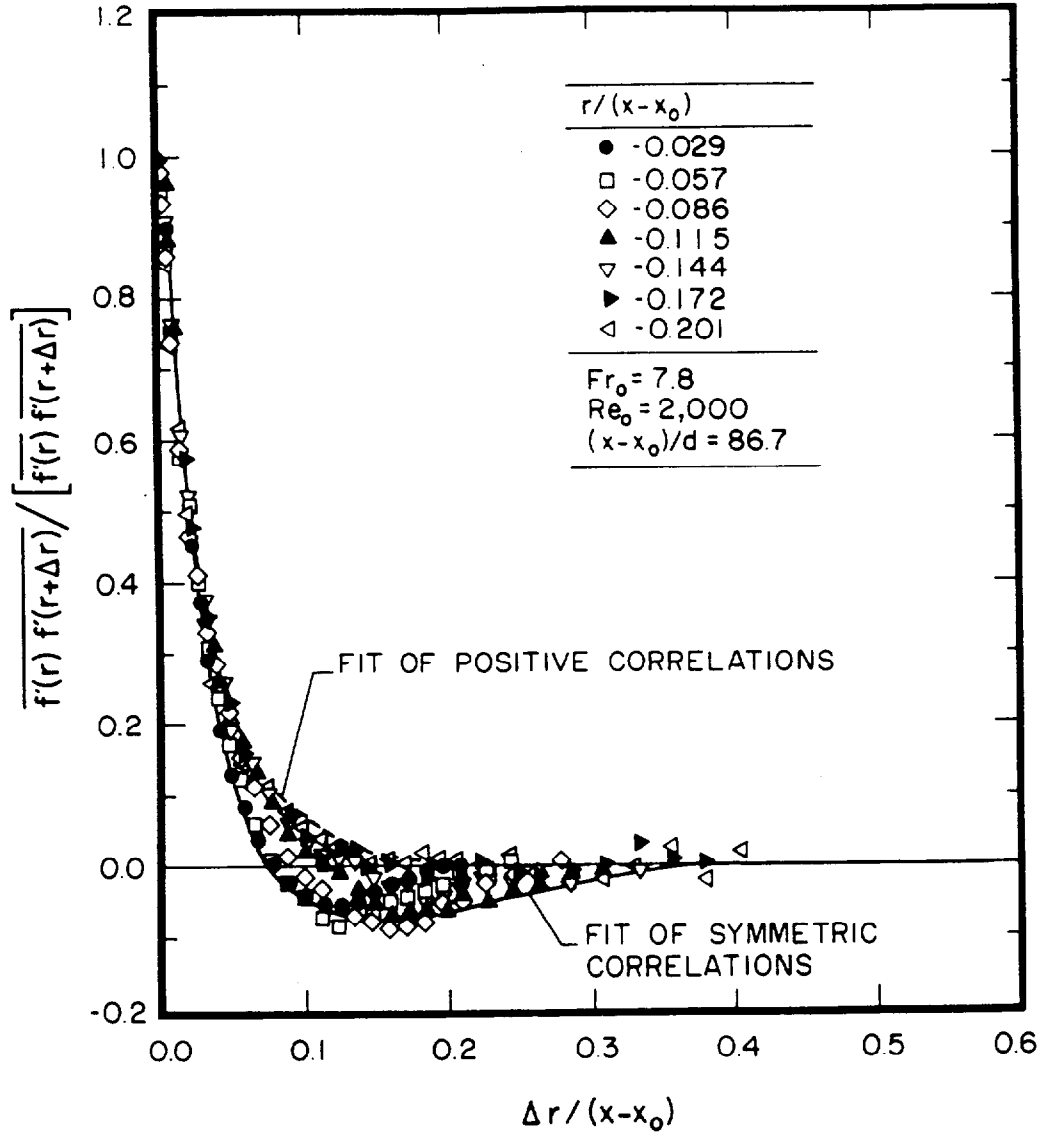


Figure 16. Negative spatial correlations of mixture fraction fluctuations

will require additional measurements of velocity and scalar flux fluctuations in order to be understood.

The final results thus far are the radial spatial integral scales for the carbon dioxide plumes in the self-preserving regime for turbulence quantities illustrated in Fig. 17. The integral scales were obtained from the correlations for positive values of r . They have been normalized by $(x-x_0)$ in Fig. 17 but measurements at other streamwise positions will be required to establish this scaling. The results indicate relatively little variation of Λ_g for $r/(x-x_0) < 0.1$, followed by a reduction toward zero at larger radial distances. This results from the intermittency of the flow at larger radial distances where the dimensions of turbulent fluid having mixture fractions greater than zero must progressively decrease. The magnitudes of the present correlations seem reasonable in comparison to existing information for jets. In particular, Becker et al. (1967) find streamwise integral scales of mixture fractions of $0.0445(x-x_0)$ within jets in comparison to present lateral integral scales of $0.035(x-x_0)$ near the axis of the plumes. Thus, present results are plausible because some differences between length scales in jets and plumes are expected while transverse correlations invariably are smaller than longitudinal or streamwise length scales in turbulent flows (Hinze, 1975).

3.4 Conclusions

Mixture fraction statistics were measured in round buoyant turbulent plumes in still air. Measurements and their interpretation are still in progress, however, the main conclusions based on results thus far can be summarized as follows:

1. Existing measurements of mean and fluctuating properties in buoyant turbulent plumes generally represent transitional plume behavior due to limited streamwise distances in comparison to source diameters and Morton length scales. Present results indicate that self-preserving conditions are reached for $(x-x_0)/d$ greater than roughly 40 and 80 for mean and turbulence properties, with $(x-x_0)/\mathcal{L}_M$ greater than 5 and 10, respectively.
2. Distributions of mean mixture fractions are narrower, with higher values at the axis, within the self-preserving region than the transitional plume results of Rouse et al. (1952) and George et al. (1977).
3. Radial profiles of mixture fraction fluctuations in the self-preserving region for turbulence properties in plumes do not exhibit reduced values near the axis similar to jets. Instead, effects of buoyancy cause mixture fractions to be maximum at the axis with intensities of roughly 45%. These large intensities probably are responsible for the large radiation fluctuation levels observed in the near-overfire region of buoyant turbulent flames (Kounalakis et al., 1991).
4. Probability density functions of mixture fractions can be approximated reasonably well by either clipped-Gaussian or beta functions. Finite levels of intermittency are observed at the axis within the self-preserving region for turbulence properties in plumes.
5. The temporal spectra of mixture fraction fluctuations are a robust property of plumes which scale in a relatively universal manner even in the transitional plume region. The spectra exhibit the well known $-5/3$ power inertial decay region followed by a -3 power inertial-diffusive region. The latter region has been observed by others in buoyant flows but is not observed in nonbuoyant flows. The

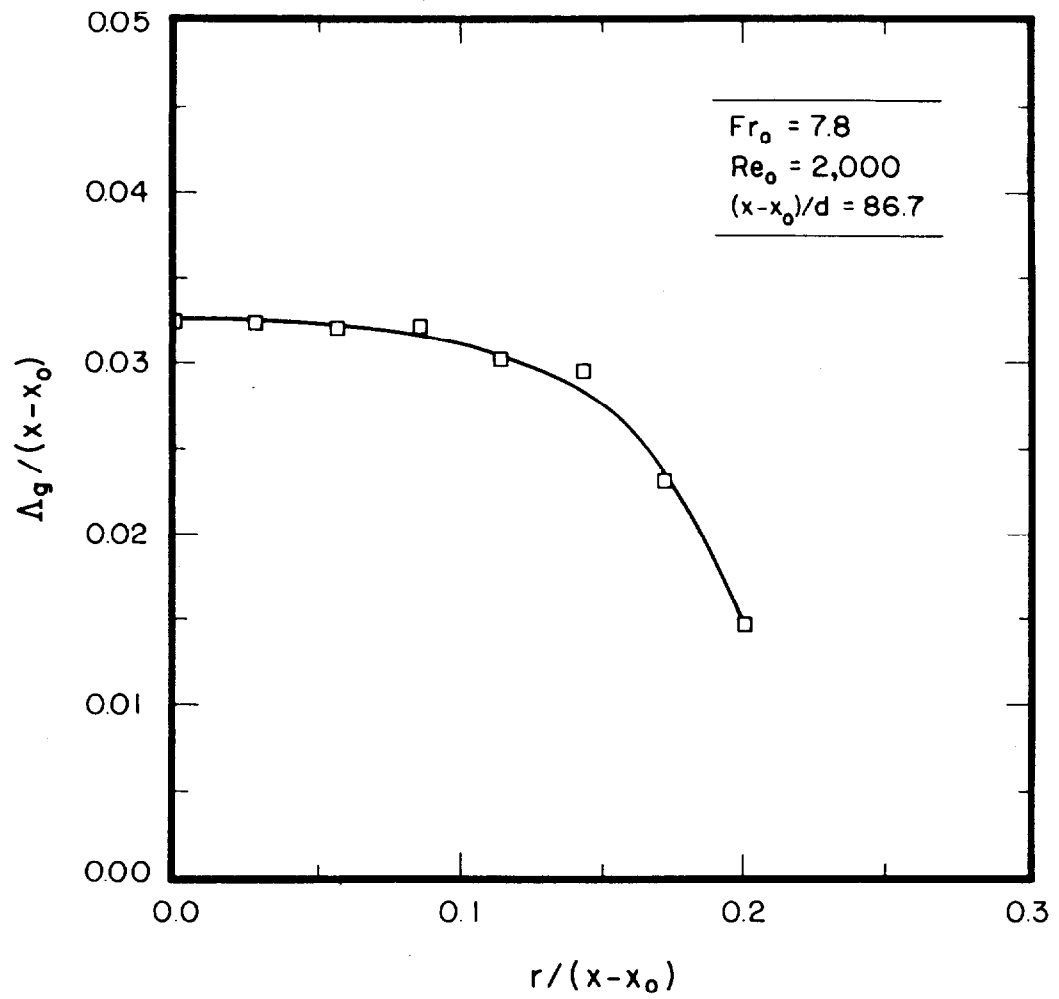


Figure 17. Radial profile of spatial integral scales

inertial-diffusive behavior is an interesting buoyancy/turbulence interaction that merits further study.

6. Radial spatial correlations were limited by correlations where both points were on the same side of the axis which exhibited an exponential decay, and symmetric correlations which approximated a Frenkiel function. This behavior probably follows from conservation of scalar flux considerations but more measurements and study are required to understand the phenomena controlling spatial correlations. Behavior near microscales was not addressed during the present study due to the limited spatial resolution of the measurements.
7. Integral scales behaved as anticipated and provisional scaling relationships have been proposed that merit additional study. Temporal integral scales were smallest at the axis which follows from Taylor's hypothesis noting that mean velocities are largest in this region. Radial spatial integral scales were largest at the axis, which follows from the topography of the flow, i.e., the streamwise extent of particular section of partially mixed turbulent fluid must decrease as the intermittency increases toward the edge of the flow.

Measurements and interpretations of data are still in progress for buoyant turbulent plumes, emphasizing self-preserving conditions for both mean and turbulence properties. These measurements include mixture fractions, velocities, and mixture fraction/velocity correlations in order to provide information needed for stochastic simulations to find turbulence/radiation interactions as well as a better understanding of buoyant turbulent flows representative of fire environments.

References

- Abraham, G. (1960) Jet diffusion in liquid of greater density. ASCE J. Hyd. Div. 86, 1-13.
- Becker, H. A., Hottel, H. C. and Williams, G. C. (1967) The nozzle-fluid concentration field of the round, turbulent, free jet. J. Fluid Mech. 30, 285-303.
- Berry, M. V. and Percival, I. C. (1986) Optics of fractal clusters such as smoke. Optica Acta 33, 577-591.
- Bohren, C. F. and Huffman, D. R. (1983) Absorption and Scattering of Light by Small Particles, Wiley and Sons, New York.
- Chang, H. Y. and Charalampopoulos, T. T. (1990) Determination of the wavelength dependence of refractive indices of flame soot. Proc. R. Soc. London A 430, 577-591.
- Chen, H. Y., Iskander, M. F. and Penner, J. E. (1990) Light scattering and absorption by fractal agglomerates and coagulations of smoke aerosols. J. Modern Optics 2, 171-181.
- Corrsin, S. and Uberoi, M. S. (1950) Further experiments on the flow and heat transfer in a heated turbulent jet. NACA Rept. 998.
- Dalzell, W. H. and Sarofim, A. F. (1969) Optical constants of soot and their application to heat flux calculations. J. Heat Trans. 91, 100-104.

- Dalzell, W. H., Williams, G. C. and Hottel, H. C. (1970) A light scattering method for soot concentration measurements. Combust. Flame 14, 161-170.
- Dobbins, R. A. and Megaridis, C. M. (1992) Absorption and scattering of light by polydisperse aggregates. Appl. Optics 30, 4747-4754.
- Erickson, W. D., Williams, G. C. and Hottel, W. C. (1964) Light scattering measurements on soot in a benzene-air flame. Combust. Flame 8, 127-132.
- George, W. K., Jr., Alpert, R. L. and Tamanini, F. (1977) Turbulence measurements in an axisymmetric buoyant plume. Int. J. Heat Mass Trans. 20, 1145-1154.
- Guinier, A. and Fournet, G. (1955) Small-Angle Scattering of X-Rays, John Wiley & Sons, New York.
- Hiller, B. and Hanson, R. K. (1990) Properties of the iodine molecule relevant to laser-induced fluorescence experiments in gas flows. Expts. Fluids 10, 1-11.
- Hinze, J. O. (1975) Turbulence, McGraw-Hill, New York, 175-319.
- Jullien, R. and Botet, R. (1987) Aggregation and Fractal Aggregates, World Scientific Publishing Co., Singapore, 46-50.
- Kerker, M. (1969) The Scattering of Light, Academic Press, New York, 414-486.
- Kotsovinos, N. E. (1985) Temperature measurements in a turbulent round plume. Int. J. Heat Mass Trans. 28, 771-777.
- Kounalakis, M. E., Sivathanu, Y. R. and Faeth, G. M. (1991) Infrared radiation statistics of nonluminous turbulent diffusion flames. J. Heat Trans. 113, 437-445.
- Köylü, Ü. Ö. (1992) Emission, structure and optical properties of overfire soot from buoyant turbulent diffusion flames. Ph.D. thesis, The University of Michigan, Ann Arbor, Michigan.
- Köylü, Ü. Ö. and Faeth, G. M. (1991a) Properties of carbon monoxide and soot emissions from buoyant turbulent diffusion flames. Report No. GDL/GMF-91-02, The University of Michigan, Ann Arbor, Michigan.
- Köylü, Ü. Ö. and Faeth, G. M. (1991b) Carbon monoxide and soot emissions from liquid-fueled buoyant turbulent diffusion flames. Combust. Flame 87, 61-76.
- Köylü, Ü. Ö. and Faeth, G. M. (1992a) Structure of overfire soot in buoyant turbulent diffusion flames at long residence times. Combust. Flame 89, 140-156.
- Köylü, Ü. Ö. and Faeth, G. M. (1992b) Radiative properties of flame-generated soot. J. Heat Trans., in press.
- Köylü, Ü. Ö. and Faeth, G. M. (1992c) Optical properties of overfire soot in buoyant turbulent diffusion flames at long residence times. J. Heat Trans., submitted.

- Köylü, Ü. Ö., Sivathanu, Y. R. and Faeth, G. M. (1991) Carbon monoxide emissions from buoyant turbulent diffusion flames. Third International Symposium on Fire Safety Science, Elsevier, London, 625-634.
- Ku, J. C. and Shim, K.-H. (1992) Optical diagnostics and radiative properties of simulated soot agglomerates. J. Heat Trans. 113, 953-958.
- Lai, M.-C. and Faeth, G. M. (1987a) Turbulence structure of vertical adiabatic wall plumes. J. Heat Trans. 109, 663-670.
- Lai, M.-C. and Faeth, G. M. (1987b) A combined laser-Doppler anemometer/laser-induced fluorescence system for turbulent transport measurements. J. Heat Trans. 109, 254-256.
- Lai, M.-C., Jeng, S.-M. and Faeth, G. M. (1986) Structure of turbulent adiabatic wall plumes. J. Heat Trans. 108, 827-834.
- List, E. J. (1982) Turbulent jets and plumes. Ann. Rev. Fluid Mech. 14, 189-212.
- Magnussen, B. F. (1974) An investigation into the behavior of soot in a turbulent free jet C_2H_2 -flame. Fifteenth Symposium (International) on Combustion, The Combustion Institute, Pittsburgh, 1415-1425.
- Martin, J. E. and Hurd, A. J. (1987) Scattering from fractals. J. Appl. Cryst. 20, 61-78.
- Mizushima, T., Ogino, F., Veda, H. and Komori, S. (1979) Application of laser-Doppler velocimetry to turbulence measurement in non-isothermal flow. Proc. R. Soc. London A366, 63-79.
- Morton, B. R. (1959) Forced plumes. J. Fluid Mech. 5, 151-163.
- Morton, B. R., Taylor, G. I. and Turner, J. S. (1956) Turbulent gravitational convection from maintained and instantaneous sources. Proc. R. Soc. London A234, 1-23.
- Nelson, J. (1989) Test of a mean field theory for the optics of fractal clusters. J. Modern Optics 36, 1031-1057.
- Ogino, F., Takeuchi, H., Kudo, I. and Mizushima, T. (1980) Heated jet discharged vertically into ambients of uniform and linear temperature profiles. Int. J. Heat Mass Trans. 23, 1581-1588.
- Papanicolaou, P. N. and List, E. J. (1987) Statistical and spectral properties of tracer concentration in round buoyant jets. Int. J. Heat Mass Trans. 30, 2059-2071.
- Puri, R. Richardson, T. F., Santoro, R. J. and Dobbins, R. I. (1992) Aerosol dynamic processes of soot aggregates in a laminar ethene diffusion flame. Combust. Flame, submitted.
- Rouse, H., Yih, C. S. and Humphreys, H. W. (1952) Gravitational convection from a boundary source. Tellus 4, 201-210.
- Rudder, R. R. and Back, D. R. (1968) Rayleigh scattering of ruby-laser light by neutral gases. J. Opt. Soc. Amer. 58, 1260-1266.

- Sivathanu, Y. R. and Faeth, G. M. (1990) Soot volume fractions in the overfire region of turbulent diffusion flames. Combust. Flame 81, 133-149.
- Sivathanu, Y. R. and Faeth, G. M. (1990b) Generalized state relationships for scalar properties in nonpremixed hydrocarbon/air flames. Combust. Flame 82, 211-230.
- Tennekes, H. and Lumley, J. L. (1972) A First Course in Turbulence. MIT Press, Cambridge.
- Tien, C. L. and Lee, S. C. (1982) Flame radiation. Prog. Energy Combust. Sci. 8, 41-59.
- van de Hulst, H. C. (1957) Light Scattering by Small Particles, Dover Publications, New York.
- Wersborg, R. L., Howard, J. B. and Williams, G. C. (1972) Physical mechanisms in carbon formation in flames. Fourteenth Symposium (International) on Combustion, The Combustion Institute, Pittsburgh, 929-940.
- Zimin, V. D. and Frik, P. G. (1977) Averaged temperature fields in asymmetrical turbulent streams over localized heat sources. Izv. Akad. Nauk. SSSR, Mekhanika Zhidkosti Gaza 2, 199-203.

NIST-114
(REV. 6-93)
ADMAN 4.09

U.S. DEPARTMENT OF COMMERCE
NATIONAL INSTITUTE OF STANDARDS AND TECHNOLOGY

MANUSCRIPT REVIEW AND APPROVAL

(ERB USE ONLY)

ERB CONTROL NUMBER	DIVISION
PUBLICATION REPORT NUMBER NIST-GCR-93-631	CATEGORY CODE
PUBLICATION DATE July 1993	NUMBER PRINTED PAGES

INSTRUCTIONS: ATTACH ORIGINAL OF THIS FORM TO ONE (1) COPY OF MANUSCRIPT AND SEND TO THE SECRETARY, APPROPRIATE EDITORIAL REVIEW BOARD.

TITLE AND SUBTITLE (CITE IN FULL)
Radiation and Mixing Properties of Buoyant Turbulent Diffusion Flames

CONTRACT OR GRANT NUMBER
60NANB1D1175

TYPE OF REPORT AND/OR PERIOD COVERED

AUTHOR(S) (LAST NAME, FIRST INITIAL, SECOND INITIAL) U.O. Koylu, Z. Dai, L.-K. Tseng and G.M. Faeth	PERFORMING ORGANIZATION (CHECK (X) ONE BOX) <input type="checkbox"/> NIST/GAITHERSBURG <input type="checkbox"/> NIST/BOULDER <input type="checkbox"/> JILA/BOULDER
--	---

LABORATORY AND DIVISION NAMES (FIRST NIST AUTHOR ONLY)

SPONSORING ORGANIZATION NAME AND COMPLETE ADDRESS (STREET, CITY, STATE, ZIP)
U.S. Department of Commerce
National Institute of Standards and Technology
Gaithersburg, MD 20899

PROPOSED FOR NIST PUBLICATION

<input type="checkbox"/> JOURNAL OF RESEARCH (NIST JRES)	<input type="checkbox"/> MONOGRAPH (NIST MN)	<input type="checkbox"/> LETTER CIRCULAR
<input type="checkbox"/> J. PHYS. & CHEM. REF. DATA (JPCRD)	<input type="checkbox"/> NATL. STD. REF. DATA SERIES (NIST NSRDS)	<input type="checkbox"/> BUILDING SCIENCE SERIES
<input type="checkbox"/> HANDBOOK (NIST HB)	<input type="checkbox"/> FEDERAL INF. PROCESS. STDS. (NIST FIPS)	<input type="checkbox"/> PRODUCT STANDARDS
<input type="checkbox"/> SPECIAL PUBLICATION (NIST SP)	<input type="checkbox"/> LIST OF PUBLICATIONS (NIST LP)	<input type="checkbox"/> OTHER _____
<input type="checkbox"/> TECHNICAL NOTE (NIST TN)	<input type="checkbox"/> NIST INTERAGENCY/INTERNAL REPORT (NISTIR)	

PROPOSED FOR NON-NIST PUBLICATION (CITE FULLY) U.S. FOREIGN

PUBLISHING MEDIUM
 PAPER CD-ROM
 DISKETTE (SPECIFY) _____
 OTHER (SPECIFY) _____

SUPPLEMENTARY NOTES

ABSTRACT (A 2000-CHARACTER OR LESS FACTUAL SUMMARY OF MOST SIGNIFICANT INFORMATION. IF DOCUMENT INCLUDES A SIGNIFICANT BIBLIOGRAPHY OR LITERATURE SURVEY, CITE IT HERE. SPELL OUT ACRONYMS ON FIRST REFERENCE.) (CONTINUE ON SEPARATE PAGE, IF NECESSARY.)

Two aspects of unwanted fires were considered: (1) the optical properties of soot in the fuel-lean region of buoyant turbulent diffusion flames, and (2) the structure and mixing properties of buoyant turbulent plumes. The scattering, absorption and extinction properties of soot were measured for conditions where soot structure was known from earlier transmission electron microscopy measurements. The measurements were compared with predictions based on the Rayleigh-Debye-Gans (RDG) scattering approximation for polydisperse fractal aggregates. The present soot aggregates exhibited significant departures from Rayleigh scattering, however, the RDG polydisperse fractal aggregate theory provided an acceptable basis to treat their optical properties. The plume study involved laser-induced iodine fluorescence measurements of mean and fluctuating mixture fractions. The results indicated that past measurements of plume properties represent transitional plumes and that self-preserving turbulent plumes are somewhat narrower, with higher levels of mean and fluctuating mixture fractions near the axis.

KEY WORDS (MAXIMUM OF 9; 28 CHARACTERS AND SPACES EACH; SEPARATE WITH SEMICOLONS; ALPHABETIC ORDER; CAPITALIZE ONLY PROPER NAMES)
diffusion flames; fire plumes; fire research; optical properties; Rayleigh light scattering; soot

AVAILABILITY <input checked="" type="checkbox"/> UNLIMITED <input type="checkbox"/> ORDER FROM SUPERINTENDENT OF DOCUMENTS, U.S. GPO, WASHINGTON, DC 20402 <input checked="" type="checkbox"/> ORDER FROM NTIS, SPRINGFIELD, VA 22161	NOTE TO AUTHOR(S): IF YOU DO NOT WISH THIS MANUSCRIPT ANNOUNCED BEFORE PUBLICATION, PLEASE CHECK HERE. <input type="checkbox"/>
--	---